

**NOVEL C₂₂H₂₄ ALKENE DIMERS FORMED VIA TITANIUM-PROMOTED REDUCTIVE DIMERIZATION
OF POLYCYCLIC CAGE KETONES. POTENTIAL NEW FUELS FOR AIRBREATHING MISSILES**

Alan P. Marchand*, M. N. Deshpande, and G. Madhusudhan Reddy

Department of Chemistry, University of North Texas, Denton, TX 76203-5068

William H. Watson* and Ante Nagl

Department of Chemistry, Texas Christian University, Fort Worth, TX 76129

INTRODUCTION

The development of new high-energy hydrocarbon fuels for use in air-breathing missiles has been the objective of a number of investigations which have received support during the past decade through programs sponsored by the Air Force Systems Command^{1,2} and/or the Naval Air Systems Command.³⁻⁵ The key characteristics which must be met by potential cruise missile fuels have been described by Burdette and coworkers.⁶ A primary requirement in this regard is that candidate fuels must possess high net volumetric heat of combustion (preferably greater than 160,000 BTU/gallon).² In order to meet the primary requirement of high net volumetric heat of combustion, hydrocarbon systems, C_nH_m, have been sought that maximize the ratio n/m. Bridged ring (polycyclic) hydrocarbon systems, by virtue of their high densities (concomitant with their compact structures), are particularly promising candidate fuels. Compounds of this type already have been utilized extensively as fuels for air-breathing missiles.

In the early stages of our study, one-pound samples of two particularly promising fuel candidates, **1** (heptacyclo[6.6.0.0^{2,6}.0^{3,13}.0^{4,11}.0^{5,9}.0^{10,14}]tetradecane, HCTD) and **2** (pentacyclo[5.4.0.0^{2,6}.0^{3,10}.0^{5,9}]undecane, PCUD, structures shown in Scheme 1) were synthesized. Both **1** and **2** display high densities (1.26 and 1.23 g-cm⁻³, respectively). The performance of each compound as a ramjet fuel has been evaluated by personnel at the Naval Weapons Center.⁷ In addition, several derivatives of **1**⁸ and of **2**⁹⁻¹¹ have been synthesized

in our laboratory.

Scheme 1

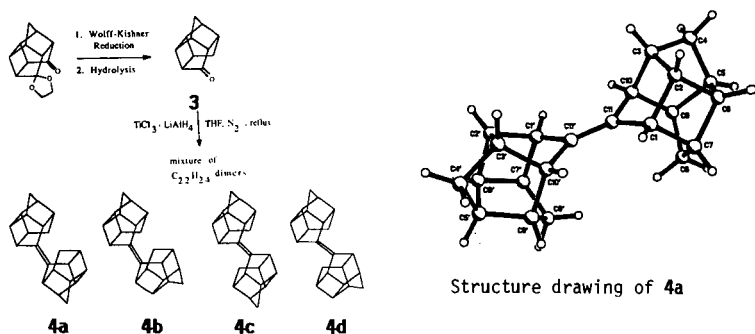


One difficulty attendant with the use of both HCTD and PCUD as fuels is their volatility. Although they are both high-melting solids, both hydrocarbons sublime readily and can escape from the binder (e.g., hydroxy-terminated polybutadiene, HTPB) on long standing at ambient temperature. In an effort to minimize the volatility of these systems (and thereby to improve their combustion and storage characteristics) without sacrificing other desirable fuel properties, we have undertaken the synthesis of HCTD and PCUD oligomers. We now report on the synthesis of some isomeric $C_{22}H_{24}$ alkenes obtained via titanium-promoted reductive dimerization¹² of polycyclic cage $C_{11}H_{20}O$ ketones and some aspects of the chemistry of the alkene dimers thereby obtained.

RESULTS & DISCUSSION

$C_{22}H_{24}$ Alkene Dimers Derived from PCUD-8-one. Our synthesis of PCUD alkene dimers, obtained via reaction of low-valent titanium with PCUD-8-one (**3**), is shown in Scheme 2. Four dimers potentially can result from this reaction, each of which possesses a twofold symmetry element (e.g., mirror plane, C_2 axis, or center of symmetry). In our hands, titanium-promoted reductive dimerization of **3** afforded a mixture of dimers, **4a-4d**, as expected. Careful fractional recrystallization of this mixture from hexane afforded a single isomer, **4a**, mp 214-215 °C, whose structure was determined via single crystal X-ray structural analysis.¹³ Particularly noteworthy is the unusually high crystal density of **4a**, i.e., 1.284 g-cm⁻³ (calculated from the X-ray data).¹³

Scheme 2



Subsequently, the remaining three isomers (i.e., **4b-4d**) were isolated by a combination of column chromatographic techniques and fractional recrystallization. Ultimately, we hope to obtain X-ray data that will permit unequivocal characterization of each of the three remaining PCUD dimers.

Recently, a study was undertaken of electrophilic additions to these PCUD dimers (individually and in the gross mixture of four dimers that results via titanium-promoted dimerization of PCUD-8-one). This was done for several reasons: First, it was of interest to determine whether structural differences among the various dimers would lead to differences in reactivity toward the electrophilic reagent, HX. If this is indeed the case, then it may be possible to separate one or possibly two of the dimers from the mixture by taking advantage of these differential reactivities. Secondly, we anticipated that Wagner-Meerwein rearrangements might occur in carbonium ion intermediates, thereby leading to the formation of interesting new C_{22} compounds that are not easily accessed via direct, titanium-promoted dimerization reactions. Finally, we are interested in determining whether or not structural differences among the various PCUD dimers might

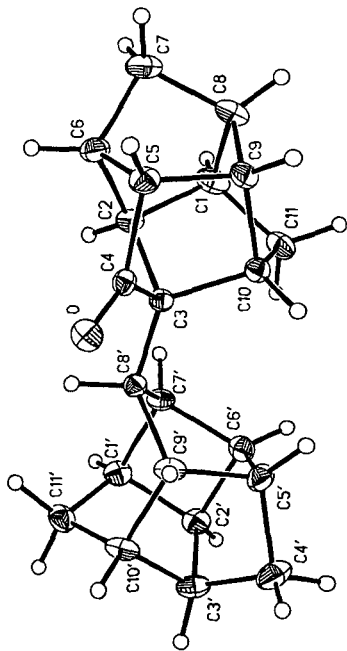
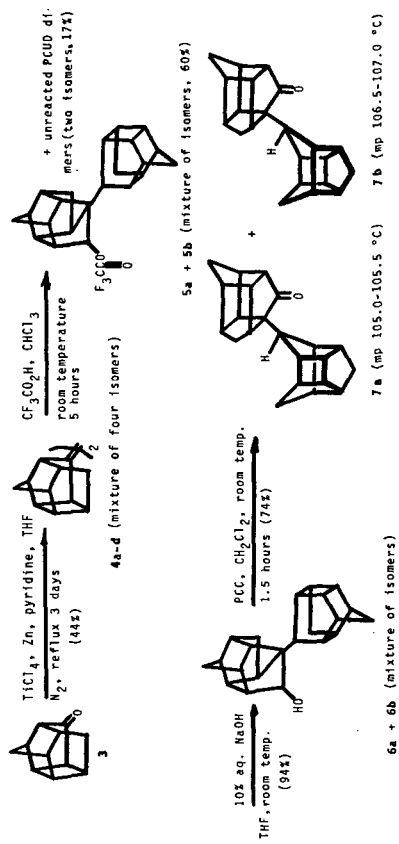
affect the mode of addition (syn vs. anti) of HX across the C=C double bond of each dimer.

The results of electrophilic addition of trifluoroacetic acid to a mixture of the four PCUD dimers (Scheme 2) are shown in Scheme 3. When the reaction with $\text{CF}_3\text{CO}_2\text{H}$ was performed at room temperature in chloroform solvent, a mixture of two trifluoroacetate adducts (**5a** and **5b**) was formed (60%) along with a mixture of two unreacted PCUD dimers (16.7%). The mixture of **5a** and **5b** was then subjected to hydrolysis with aqueous base, thereby affording a mixture of alcohols, **6a** and **6b**. The resulting mixture of alcohols was oxidized subsequently by using pyridinium chlorochromate (PCC) in methylene chloride solvent. The product was found to be a mixture of two isomeric ketones, **7a** and **7b**, which could be separated by flash column chromatography. The structures of **7a** and **7b** each have been established unequivocally by single crystal X-ray structural analysis.¹⁴

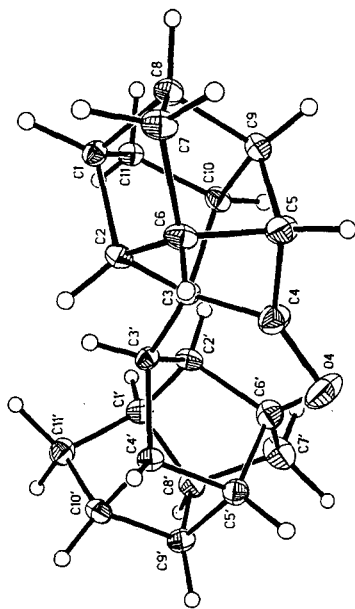
Subsequently, the unreacted dimer (recovered from the above reaction; mixture of two isomers) was treated with trifluoroacetic acid in refluxing chloroform. Addition of trifluoroacetic acid to the C=C double bond in the mixture of dimers occurred under these conditions. Basic hydrolysis of the trifluoroacetate adduct followed by oxidation with PCC again afforded a mixture of **7a** and **7b**.

Recently, we have studied the Wolff-Kishner reduction of isomerically pure ketones **7a** and **7b**. Of particular interest is the fact that the hydrocarbons thereby obtained differ substantially in melting point. The product of Wolff-Kishner reduction of **7a** (i.e., **8a**) displays mp 114-115 °C, whereas the corresponding product obtained by Wolff-Kishner reduction of **7b** (i.e., **8b**) displays mp 74-75 °C. The structure of **8a** has been determined by X-ray crystallographic methods (Scheme 4); the calculated crystal density of **8a** was found to be 1.290 g-cm⁻³.¹⁵

Scheme 3

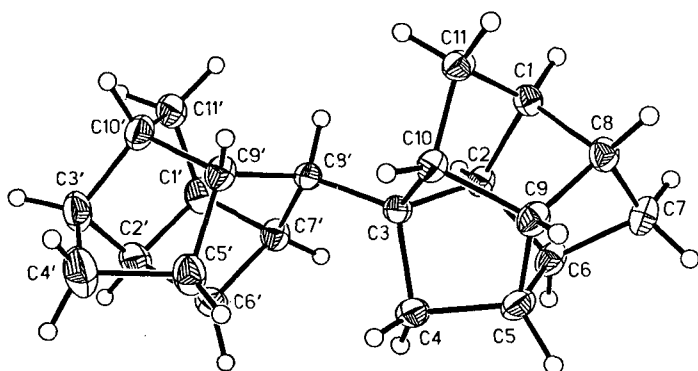


Structure drawing of 7a



Structure drawing of 7b

Scheme 4

Structure drawing of **8a**

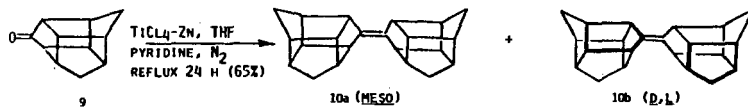
C₂₂H₂₄ Alkene Dimers Derived from D₃-Trishomocubanone. As an extension of the foregoing study, alkene dimers have been synthesized via titanium-promoted reductive dimerization of the D₃-trishomocubanone (**9**). In this case, only two dimers [i.e., **10a** (*meso*) and **10b** (*d_xl*)] can result from this reaction (Scheme 5). Indeed, a 1:1 mixture of **10a** and **10b** was obtained from this reaction. Careful fractional recrystallization of the mixture of dimers thereby obtained from ligroin afforded a single isomer, mp 246 °C. This dimer was shown to possess the *meso* configuration (i.e., **10a**) by single crystal X-ray structural analysis.¹⁶ Of particular significance is the unusually high calculated crystal density of **10a**, i.e., 1.302 g·cm⁻³.

More recently, the corresponding *d_xl* dimer, **10b**, mp 186 °C, has been isolated, and its structure has been determined by X-ray crystallographic methods (Scheme 5). Interestingly, the calculated crystal density of **10b** (1.269 g·cm⁻³) is significantly lower than that of **10a**.¹⁶

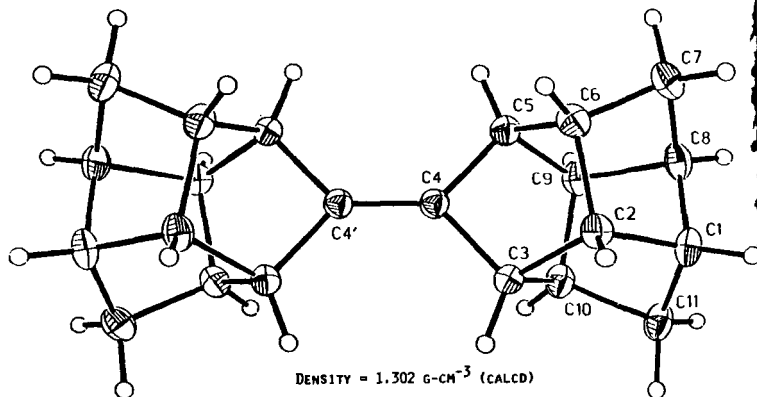
Two important results of that have emerged from the studies described above are

Scheme 5

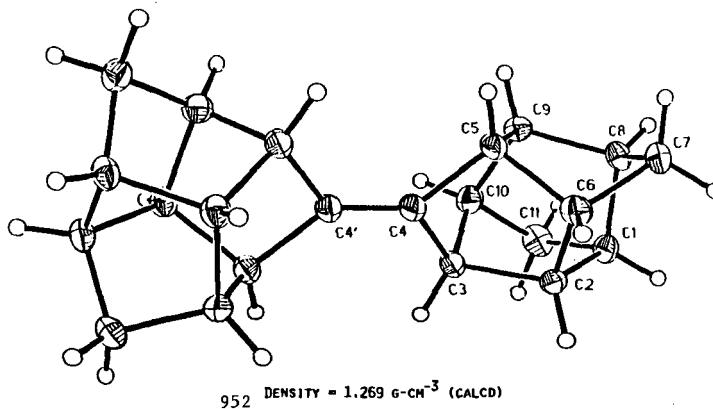
DIMERS DERIVED FROM D₃-TRISHOMOCUBANONE



Structure drawing of 10a



Structure drawing of 10b



noteworthy. First, the calculated crystal densities of PCUD dimer **4a**, of the rearranged cage hydrocarbon **8a**, and of **10a** and **10b** (i.e., 1.284, 1.290, 1.302, and 1.269 g-cm⁻³, respectively) rank among the highest known hydrocarbon densities; [compare these values with the densities of cubane (1.29 g-cm⁻³),¹⁷ 1,16-dimethyldodecahedrane (1.412 g-cm⁻³)¹⁸ and dodecahedrane (1.448 g-cm⁻³)¹⁹].

Second, it is important to note that all of the three dimeric alkenes, i.e., **4a**, **10a**, and **10b**, whose X-ray crystal structures have been determined thus far in our study, are all C₂₂H₂₄ isomers that possess distinctly different crystal densities. Any of the existing calculational methods that are used to estimate crystal densities are based upon molecular formula and functional group additivity and therefore are incapable of predicting variations in densities among geometric isomers.²⁰ Hence, contrary to the X-ray crystallographic results cited above, all of our C₂₂H₂₄ isomers are predicted by any of these methods to possess the same density.

SUMMARY & CONCLUSIONS

Our efforts to synthesize oligomers of strained polycyclic cage monomers have resulted in the synthesis of novel cage alkene dimers **4a-4d**, **10a** and **10b**, along with derivatives of these systems. These dimers possess unusually high crystal densities and are relatively nonvolatile; both properties are considered to be desirable for new candidate fuel systems. The electrophilic addition of trifluoroacetic acid to a mixture of PCUD alkene dimers, **4a-4d**, has been studied, and several reaction products have been characterized by single crystal X-ray structural analysis. Future studies will be directed toward: (i) the synthesis of oligomers of HCTD (**1**) and (ii) studies of reactions of **10a** and **10b** with a variety of electrophiles.

ACKNOWLEDGMENTS

We thank the Air Force Office of Scientific Research (Grant AFOSR-88-0132), the Robert A. Welch Foundation (Grant B-963 to A. P. M. and Grant P-074 to W. H. W.), the National Science Foundation (CHE-8514367 to W. H. W.) and the University of North Texas and the Texas Christian University Faculty Research Committees for financial support of this research.

REFERENCES AND FOOTNOTES

1. Schneider, A.; Janoski, E. J.; Moore, R. E.; Ware, R. E. Air Breathing Missile Fuel Development, U. S. Air Force Aero Propulsion Report No. AFAPL-TR-74-44, May, 1974.
2. Schneider, A.; Janoski, E. J.; Lyons, J. E.; Myers, H. K. Air Breathing Missile Fuel Development, U. S. Air Force Aero Propulsion Report No. AFAPL-TR-74-44, Volume III, November, 1976.
3. Burdette, G. W.; Bryant, J. T. Ramjet Fuel Studies, Part 3, Liquid Hydrocarbons, Naval Weapons Center Report No. NWC-TP-4810, Part 3, January, 1977.
4. Burdette, G. W.; Bryant, J. T.; Wood, S. E. Investigation of New Liquid Hydrocarbon Fuels for Ramjets and Liquid Propellant Guns, Naval Weapons Center Technical Memorandum No. 2887, August, 1976.
5. Burdette, W.; Reed, R., Jr. Navy High Energy Solid Ramjet Fuel Program, 1979 JANNAF Propulsion Symposium, Anaheim, California, 5-9 March 1979.
6. Burdette, G. W.; Lander, H. R.; McCoy, J. R. J. Energy, **1978**, 2, 289.
7. Burdette, G. W.; Schadow, K. unpublished results.
8. Marchand, A. P.; Wu, A.-h. J. Org. Chem., **50**, 396 (1985).
9. Marchand, A. P.; Suri, S. C.; Earlywine, A. D.; Powell, D. R.; van der Helm, D. J. Org. Chem., **1984**, 49, 670.
10. Marchand, A. P.; Kaya, R.; Baker, A. D. Tetrahedron Lett., **1984**, 25, 795.
11. Marchand, A. P.; Huang, C.; Kaya, R.; Baker, A. D.; Jemnis, E. D.; Dixon, D. A. J. Am. Chem. Soc., **1987**, 109, 7095.
12. For a review of titanium-induced dicarbonyl-coupling reactions, see: McMurry, J. E. Acc. Chem. Res., **1983**, 16, 405.
13. Flippen-Anderson, J. L.; Gilardi, R.; George, C.; Marchand, A. P.; Jin, P.-w.; Deshpande, M. N. Acta Cryst., Sect. C.: Cryst. Struct. Commun. **1988**, C44, 1617.
14. Watson, W. H.; Nagl, A.; Marchand, A. P.; Deshpande, M. N. Acta Cryst., Sect. C: Cryst. Struct. Commun. **1989**, C45, 0000.
15. Watson, W. H.; Nagl, A.; Marchand, A. P.; Deshpande, M. N. Acta Cryst., Sect. C: Cryst. Struct. Commun. Manuscript in preparation.
16. Marchand, A. P.; Reddy, G. M.; Deshpande, M. N.; Watson, W. H.; Nagl, A.; Lee, D. S.; Osawa, E. Manuscript in preparation.
17. (a) Fleischer, E. B. J. Am. Chem. Soc., **1964**, 86, 3889; (b) Eaton, P. E. personal communication.
18. Christoph, C. G.; Engel, P.; Usha, R.; Balogh, D. W.; Paquette, L. A. J. Am. Chem. Soc., **1982**, 104, 784.
19. Gallucci, J. C.; Doecke, C. W.; Paquette, L. A. J. Am. Chem. Soc., **1986**, 109, 1343.
20. Amnon, H. L.; Z. Du Acta Cryst., Sect. C: Cryst. Struct. Commun. **1988**, C44, 1059.

MODELING OF THE THERMAL STABILITY OF AVIATION FUELS

G.V. Deshpande, Michael A. Serio, Peter R. Solomon, and Ripudaman Malhotra*

Advanced Fuel Research, Inc.
87 Church Street
East Hartford, CT 06108

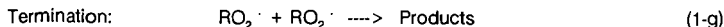
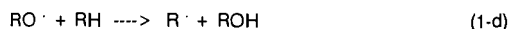
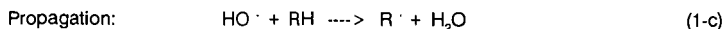
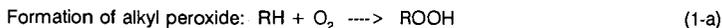
*SRI International
333 Ravenswood Avenue
Menlo Park, CA 94025

INTRODUCTION

The detailed chemical reactions that result in fuel deposits are very complex and very poorly understood at the present. However, it has been reported by several researchers (1-6) that the reaction usually initiates with a liquid phase oxidation of the fuel, which is promoted by dissolved oxygen. Common impurities such as compounds of sulfur, nitrogen, and dissolved metals play a role by either accelerating the reactions or affecting the solubility of the degradation products. Above 750 K, the deposition reaction is characterized by the pyrolysis of hydrocarbon molecules and the scission of hydrogen.

Mayo and Lan (2) have studied the rates of oxidation and gum formation for different fuels. They used $t\text{-BU}_2\text{O}_2$ as the initiator and found that some fuels oxidized faster at 100°C than in their previous work (7) at 130°C without initiator. They proposed that gum formation starts with coupling of two alkyl peroxy radicals in the chain termination of oxidation and that growth beyond dimer depends on converting dimer to peroxy radicals by chain propagation.

The general free radical mechanism agreed upon by several researchers and outlined by Foder et. al. (5) is given below.



A study was done at Advanced Fuel Research, Inc. (AFR) in which Fourier Transform Infrared Spectroscopy (FT-IR) and Field Ionization Mass Spectrometry (FIMS) were used to study the products from fuel degradation (soluble gums, insoluble gums, and deposits removed on a wire collection probe) (8). The results indicated that the wire deposits were primarily long chain aliphatics (heavier than the starting fuel), which may be formed by termination steps in the above mechanism. The soluble gums were primarily lower molecular weight aliphatics and aromatics which are likely formed by the main decomposition steps. The insoluble gums were intermediate in character, although more closely resembled the wire deposits.

A detailed thermal stability model will require study of additional fuels over a wide range of conditions. A preliminary global model was developed to describe the processes influencing deposition by extending work done at the United Technologies Research Center (UTRC) (4). The UTRC model employed two steps to describe decomposition, step 1 in which fuel plus oxygen is converted into a precursor for deposit formation and step 2 in which the precursor is converted to deposit. We have added a third step for the decomposition of the precursor back to fuel and CO₂. In addition, we have added a mass transport step which can limit the transport of the precursor to the wall surfaces.

MODEL DEVELOPMENT

Because of the difficulty in applying the detailed deposition mechanism cited in Eqs. (1-a) through (1-h) to a multi-component fuel, global reaction mechanisms are often postulated. A global model is also more appropriate for input into a comprehensive code which also includes fluid mechanics and heat transfer.

A two-step kinetic reaction mechanism has been postulated by Giovanetti and Szetela (4) and has been successfully applied to a number of time-temperature histories of the jet fuels. There are two major drawbacks of the model: 1) It does not consider any mass transfer effects; 2) It does not have possible precursor decomposition reactions which will be relevant at high temperatures.

Marteney and Spadaccini (9) have reported deposition rates for a wide temperature range and have found that at temperatures above 645 K, there is a sudden decrease in the deposition rate. A similar trend has been found by Taylor (10). This sudden drop could be due to possible mass transfer resistances at high temperatures and/or precursor decomposition. Marteney and Spadaccini (9) also studied the effect of fuel flow rate on the deposition rate. They found that the peak deposition rate occurred at a lower temperature in laminar flow, suggesting that the reaction became mixing limited at elevated temperatures.

Clark and Thomas (11) found evidence that a fuel's behavior in the JFTOT may be dominated by physical transport or chemical reaction processes and that the relative importance of these two factors is fuel dependent. They found that the weight of the carbon deposited per unit flow rate went through a maximum as the flow rate was increased from 1 ml/min to 11 ml/min. They have explained their results by 3 possible rate limiting steps and postulated that the time constant of each step is fuel and flow rate dependent.

The following summary can be made of the observations on field deposition from the experimental data reported in literature.

1. The deposition rate goes through a maximum with temperature.
2. The deposition rate goes through a maximum with length of the tube.
3. The deposition rate at low temperatures declines with prestressing.
4. The deposition rate at high temperatures does not change with prestressing.
5. The pressure does not appear to exert any influence on the deposition rate.
6. The deposition rate changes with flow rate and time of the experiment. Based on these observations the following global fuel oxidation and deposition model is proposed.



It is assumed that reactions 2-a and 2-b occur in the bulk and reaction 2-c occurs on the inner wall surface. For laminar flow, a stagnant layer exists in the vicinity of the wall and the mass transfer resistance may be significant for the precursor.

The time rates of change of the active species are given by

$$d[\text{O}_2]/dt = -K_1 [\text{fuel}] [\text{O}_2] \quad (3-a)$$

$$d[\text{precursor}]/dt = K_1 [\text{fuel}] [\text{O}_2] - K_3 [\text{precursor}] [\text{fuel}] - R_m \quad (3-b)$$

$$d[\text{deposit}]/dt = K_2 [\text{fuel}] [\text{precursor}]_s \quad (3-c)$$

where the brackets [] denote concentration in moles/cc and the subscript s denotes the concentration at the inner surface of the tube. The mass transfer rate, R_m is given by

$$R_m = K_m \cdot S \cdot ([\text{precursor}] - [\text{precursor}]_s) \quad (4-a)$$

where K_m is the mass transfer coefficient (cm/sec) and s is surface area per unit volume (cm^{-1})

$$S = 4/d \quad (4-b)$$

where d is the inner diameter of the tube.

If we equate the mass transfer rate to the deposition rate (assuming steady state), we get

$$R_m = K_{\text{EFF}} \cdot [\text{precursor}] \quad (4-c)$$

where K_{EFF} is given by the following equation

$$1/K_{\text{EFF}} = 1/K_2/[\text{fuel}] + d/4/K_m \quad (4-d)$$

The mass transfer coefficient, K_m is estimated by using heat transfer analogy.

The Nusselt number for heat transfer for laminar flow is given by the Seider-Tate equation (12). The Nusselt number for mass transfer can be written as

$$\text{Nu}_{\text{AB}} = 1.86 \text{Re}^{1/3} \text{Sc}^{1/3} (d/L)^{1/3} \quad (5-a)$$

where Re and Sc are the Reynolds and Schmidt numbers, respectively, and L is the length of the tube.

Marteny and Spadaccini (9) have given the heat transfer characteristics of JP-5 and found that for the transition and turbulent region, a simple Dittus-Boelter equation could be used to describe the heat transfer characteristics.

Thus for the non-laminar region, the Nusselt number for mass transfer can be written as

$$Nu_{AB} = 0.023 Re^{0.8} Pr^{0.4} \quad (5-b)$$

The mass transfer coefficient, K_m is then given by the following equation

$$K_m = Nu_{AB} \cdot D^*_{AB}/d \quad (5-c)$$

where D^*_{AB} is the binary diffusivity of the precursor-fuel system.

The binary diffusivity can be estimated by Wilke and Chang (13,14) as follows

$$D^*_{AB} = \frac{(117 \cdot 3 \times 10^{-18}) (Q M_B)^{0.5} T}{\mu \nu_A^{0.6}} \quad (6)$$

where D^*_{AB} = diffusivity of A in very dilute solution in Solvent B, m^2/s , M_B = molecular weight of solvent, kg/kmol, T = temperature, K, μ = solution viscosity, kg/m \cdot s, ν_A = solute molar volume at normal boiling point, $m^3/kmol$, Q = association factor for solvent and is 1.0 for unassociated solvents. ν_A can be estimated from the molecular formula of the diffusing species and the values of atomic and molecular volumes (15).

MODEL PREDICTIONS

The experimental data used in the modeling has been taken from the NASA report by Giovanetti and Szetela (4). As discussed above, they had proposed a two-step reaction model. Their model curves are compared with the experimental data for three cases in Figs. 1a, 2a, 3a, respectively. The experimental data of Fig. 2a was used to calibrate the model and hence the fit to it is the best of the three cases. There was a discrepancy in the UTRC model. In order to fit the data, the initial oxygen concentration in fuel was assumed to be 16% of the saturation value. In addition, the mass transfer effects and precursor decompositions, which yield lower deposit formation rates at high temperatures were also neglected.

The results of the simulation of the model which included mass transfer effects are shown in Figs. 1b, 2b, and 3b. It can be seen that the model underpredicts the deposit formation at high temperatures where mass transfer effects are likely to be important. At low temperature, the model predictions are slightly improved. Thus even at the low temperature, some mass transfer resistance is present due to the very low velocity used in this experiment.

When the model constants were fitted in the UTRC work, the mass transfer effects were neglected and hence the frequency factor and activation energy for the deposit formation reaction were the global rate instead of the true kinetic rate. Consequently, in order to fit the data with mass transfer, the frequency factor or activation energy had to be changed. In addition, the initial oxygen concentration was made equal to the saturation value. The frequency factor of the reaction for deposit formation was kept constant and the activation energy was increased from 31,000 kcal/mole to 32,600 kcal/mole. The results of these simulations are given in Figs. 1c, 2c, and 3c, respectively. By this change, the experimental data at low temperature (low velocity) and high temperature (high velocity) were predicted

very well but the data at high temperature (low velocity) showed a leveling effect after distance of 60 cm and the model predicted an increasing trend of deposit formation even at distance of 120 cm.

The above observation suggested that the leveling off of the deposit formation is due to the precursor decomposition. This would also explain the trend of lower deposit formation at higher temperatures. A third reaction of precursor decomposition was incorporated in the model with the activation energy of 32,600 and frequency factor of 2.0×10^{14} . The results of these simulations are given in Fig. 1d, 2d, and 3d, respectively. **The model now seems to predict the data very well for all the three cases.**

Giovanetti and Szetela (4) have also measured the deposit formation for the fuel Suntech A. The major differences between fuel Jet A and the fuel Suntech A are in the organic oxygen content, the aromatic and paraffins content and in the amount of trace elements. Based on the speculations of the various researchers reported in literature, Suntech A would be more reactive fuel than Jet A and consequently deposit formation will be higher than Jet A under identical stressing conditions. This kind of behavior was found by Giovanetti and Szetela (4) and it was reported that the carbon deposition rates for Suntech A were as high as a factor of ten greater than those for Jet A.

The UTRC model and the AFR model were exercised over two time-temperature histories for Suntech A. The deposit formation was underpredicted, which is attributed to the higher reactivity of Suntech A than Jet A. The fuel reactivity would influence the rate of the precursor formation and possibly of deposit formation. Hence the rates of these reactions were increased 40 times by increasing the frequency factor. The results of these simulations are shown in Figs. 4a and 4b. The low temperature deposit formation is predicted very well but the high temperature data are underpredicted.

Since Suntech A had a higher organic oxygen content than Jet A and the chemical composition was different (i.e. more aromatic than Jet A), the oxygen solubility and/or initial precursor concentration could be different. In our model, the initial precursor concentration is assumed to be zero. Hence the initial oxygen concentration was doubled and the rates of precursor and deposit formation were increased 20 times in the Jet A parameters. The results of these simulations are shown in Figs. 4c and 4d. The low temperature data is predicted equally well but the predictions at high temperatures are greatly improved. This result suggests that the knowledge of precursor concentration in the fuel may be important and the deposit formation may be greatly enhanced if the oxygen solubility in the fuel is higher and/or the fuel contains oxygenated species to begin with.

Sensitivity Analysis - The AFR model is a three reaction model which also includes mass transfer effects. A preliminary sensitivity analysis for the reaction parameters was done by varying the frequency factor so that the rate constants were increased by an order of magnitude on either side of the base case. The mass transfer effects were studied by varying the diffusivity.

(a) Variations in Diffusivity - This was achieved by varying the constant in the Stokes-Einstein (16) equation ($D_{AB}\mu_B/T = \text{Constant}$). The base case used for the sensitivity analysis was that of fuel Jet A under high temperature and low velocity conditions where the mass transfer effects will have the maximum impact on deposit formation. Since the binary diffusivity of the precursor in the fuel is estimated by correlation, the sensitivity of this estimation was done and is shown in Fig. 5a. **The effect of increasing the diffusivity significantly increases the amount of deposit formation and this clearly shows the base case chosen is mass transfer limited as expected.**

(b) Variations in A(1) - The rate constant, K_1 , of the reaction forming precursor was varied by varying the frequency factor. The results are shown in Fig. 5b. It is interesting to note that lowering the rate constant by an order of magnitude results in significantly lowering the amount of deposit formation but increasing by an order of magnitude does not change the amount of deposit formation very much. **This suggests that the precursor formation rate is not always limiting the deposition process.**

(c) Variations in A(2) - The rate constant, K_2 , of the reaction forming deposit was varied by varying the frequency factor. The results are shown in Fig. 5c. An effect similar to that observed for the variation of K_1 is seen for variation of K_2 . Even though K_2 was increased by an order of magnitude, the amount of deposit formation did not increase very much. This reinforces the fact that the base case is mass transfer limited. Lowering of K_2 , however, did decrease the amount of deposit formation.

(d) Variations in A(3) - The rate constant, K_3 , of the reaction involving precursor decomposition was varied by varying the frequency factor. The results are shown in Fig. 5d. Since increasing this rate reduces the precursor concentration, the deposit formation is reduced. Lowering the rate by an order of magnitude does not increase the deposit formation by a large amount but increasing the rate did decrease the deposit formation.

Predictions of AFR Data - The results shown in Fig. 6 show that the model can predict the maximum in deposit measured in our experiments (8,17). This maximum cannot be predicted by the UTRC model.

SUMMARY

A preliminary global model was developed extending the work done at UTRC. This new model which includes mass transfer and a precursor decomposition step can predict variations in deposit formation with fuel type, flow rate, residence time, and temperature-time history. This initial modeling effort has indicated that the measurement of the deposit precursors in addition to the deposit formation is clearly needed for model discrimination purposes. The use of on-line FT-IR diagnostics used in a related study (8,17) will help to identify the different precursors and their concentration behavior with temperature and residence time.

ACKNOWLEDGEMENTS

The authors wish to acknowledge the support of the U.S. Air Force (Aero Propulsion Laboratory, Wright Aeronautical Laboratories, Aeronautical Systems Division, Wright-Patterson AFB, Ohio) under Contract No. F33615-88-C-2853. We are also grateful to Dr. Pierre Marteny of the United Technologies Research Center (UTRC), East Hartford, CT who supplied copies of past UTRC reports on modeling of thermal stability.

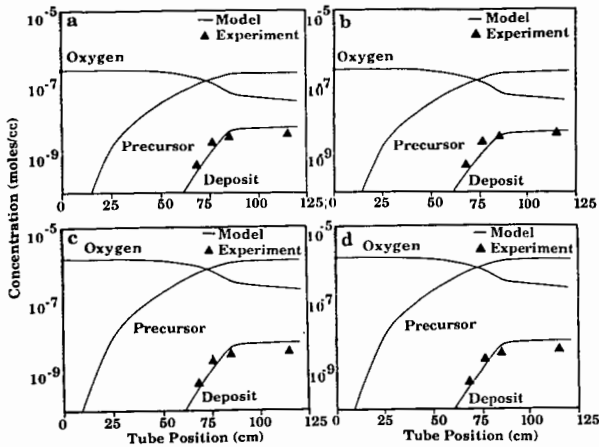


Figure 1. Predicted and Measured Deposit Species Concentration - Tube Position Histories for Jet A Flowing in a Heated Tube - Low Temperature and Low Velocity Condition. a) UTRC Model (O_2 init = 2.25×10^{-7} moles/cc, $E(2) = 31,000$ cal/gmole, $E(3) = 0$ cal/gmole), b) AFR Model (O_2 init = 2.25×10^{-7} moles/cc, $E(2) = 31,000$ cal/gmole, $E(3) = 0$ cal/gmole), c) AFR Model (O_2 init = 1.40×10^{-6} moles/cc, $E(2) = 32,600$ cal/gmole, $E(3) = 0$ cal/gmole), and d) AFR Model (O_2 init = 1.40×10^{-6} moles/cc, $E(2) = 32,600$ cal/gmole, $E(3) = 32,600$ cal/gmole). Data from Ref. 4.

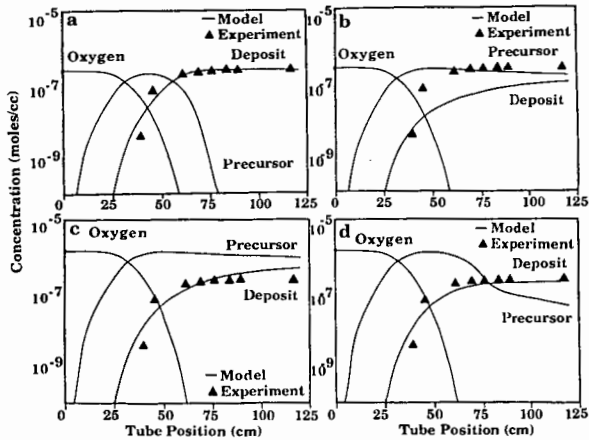


Figure 2. Predicted and Measured Deposit Species Concentration - Tube Position Histories for Jet A Flowing in a Heated Tube - High Temperature and Low Velocity Condition. a) UTRC Model (O_2 init = 2.25×10^{-7} moles/cc, $E(2) = 31,000$ cal/gmole, $E(3) = 0$ cal/gmole), b) AFR Model (O_2 init = 2.25×10^{-7} moles/cc, $E(2) = 31,000$ cal/gmole, $E(3) = 0$ cal/gmole), c) AFR Model (O_2 init = 1.40×10^{-6} moles/cc, $E(2) = 32,600$ cal/gmole, $E(3) = 0$ cal/gmole), and d) AFR Model (O_2 init = 1.40×10^{-6} moles/cc, $E(2) = 32,600$ cal/gmole, $E(3) = 32,600$ cal/gmole). Data from Ref. 4.

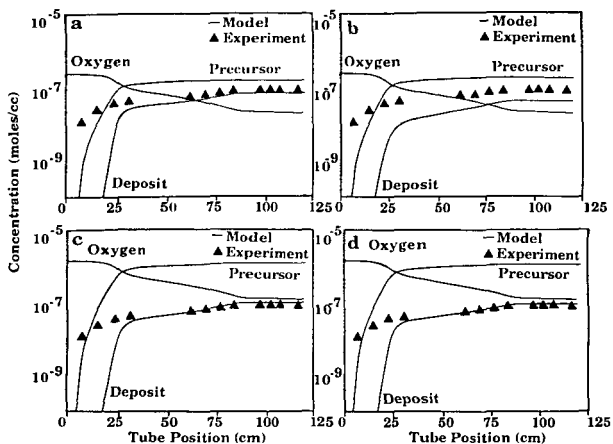


Figure 3. Predicted and Measured Deposit Species Concentration - Tube Position Histories for Jet A Flowing in a Heated Tube - High Temperature and High Velocity Condition. a) UTRC Model (O_2 init = $2.25E-7$ moles/cc, $E(2) = 31,000$ cal/gmole, $E(3) = 0$ cal/gmole, b) AFR Model (O_2 init = $2.25E-7$ moles/cc, $E(2) = 31,000$ cal/gmole, $E(3) = 0$ cal/gmole, c) AFR Model (O_2 init = $1.40E-6$ moles/cc, $E(2) = 32,600$ cal/gmole, $E(3) = 0$ cal/gmole, and d) AFR Model (O_2 init = $1.40E-6$ moles/cc, $E(2) = 32,600$ cal/gmole, $E(3) = 32,600$ cal/gmole. Data from Ref. 4.

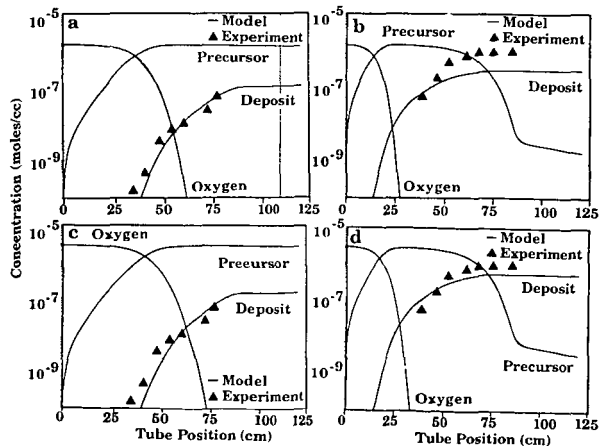


Figure 4. Predicted and Measured Deposit Species Concentration - Tube Position Histories for Suntech A Flowing in a Heated Tube - Low Velocity Condition. $E(1) = 17,000$ cal/gmole, $E(2) = 32,600$ cal/gmole, $E(3) = 32,600$ cal/gmole and $A(3) = 0.2 E15$. a and c are Low Temperature and b and d are High Temperature Conditions. a and b) (O_2 init = $1.40E-6$ moles/cc, $A(1) = 0.14E12$, $A(2) = 0.8E16$ and c and d) (O_2 init = $2.80E-6$ moles/cc, $A(1) = 0.07E12$, $A(2) = 0.4E16$. Data from Ref. 4.

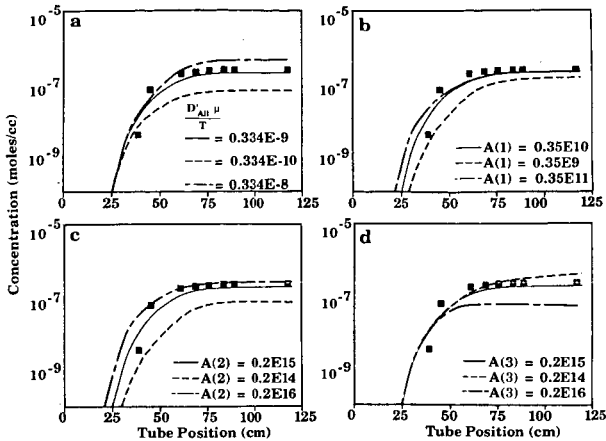


Figure 5. Effect on Deposit Formation of: a) Diffusivity, D_{AB} , b) Rate Constant, k_1 , c) Rate Constant, k_2 , and d) Rate Constant, k_3 for Fuel Jet A under High Temperature and Low Velocity Conditions. Base Case: $D_{AB}\mu/T = 0.334E-9$, $A(1) = 0.35E10$, $A(2) = 0.2E15$, $A(3) = 0.2E15$. Data from Ref. 4.

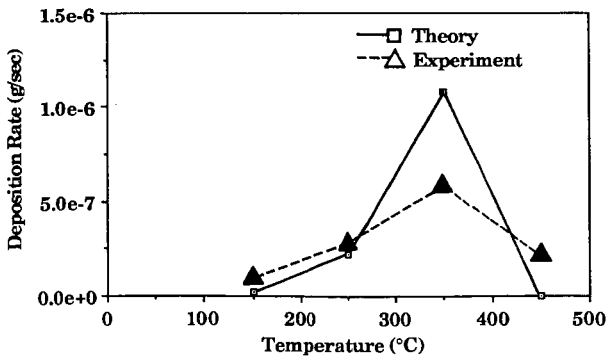


Figure 6. Comparison of AFR Model Predictions with Deposition Rate for Aerated JP-5.

REFERENCES

1. Kendall, D.R. and Mills, J.S., *Ind. Eng. Chem. Prod. Res. Dev.*, **25**, 360 (1986).
2. Hazlett, R.N., "Free Radical Reactions Related to Fuel Research," in Frontiers of Free Radical Chemistry, William A. Pryor (Ed.), Academic Press, New York, pp. 195-223 (1980).
3. Mayo, F.R. and Lan, B.Y., *Ind. Eng. Chem. Res.*, **25**, 333, (1986).
4. Giovanetti, A.J., and Szetela, E.J., "Long Term Deposit Formation in Aviation Turbine Fuel at Elevated Temperature", NASA Final Report, Contract No. NAS3-24091, (1985).
5. Fodor, G.E., *Energy and Fuel*, **2**, 729, (1988).
6. Reddy, K.T. and Cerransky, N.P., *Energy and Fuel*, **2**, 205, (1988).
7. Tseregounis, S.I., Spearot, J.A. and Kite, D.J., *Ind. Eng. Chem. Res.*, **26**, 886 (1987).
8. Serio, M.A., Malhotra, R., Kroo, E., Desphande, G.V., Solomon, P.R., "A Study of the Thermal Stability of JP-5 using FT-IR and FIMS" paper to be presented at the Symposium on the structure of Future Jet Fuels II, Division of Petroleum Chemistry, ACS Miami Meeting, Sept. 10-15, 1989.
9. Marteney, P.J. and Spadaccini, L.J., *Journal of Eng. For Gas Turbines and Power*, **108**, 648, (1986).
10. Taylor, W.F., *IEC Product Res. Dev.*, **8**, 375, (1965).
11. Clark, R.H. and Thomas, L., "An Investigation of the Physical and Chemical Factors Affecting the Performance of Fuels in The JFTOT", presented at the SAE Aerospace Technology Conf. and Exposition, Anaheim, CA, (1988).
12. Sieder, E.N. and Tate, G.E., *Ind. Eng. Chem.* **28**, 1429, (1936).
13. Wilke, C.R., *Chem. Eng. Progr.*, **45**, 218, (1949).
14. Wilke, C.R., and Chang, P., *AIChE, J.*, **1**, 264, (1965).
15. Treybal, R.E., Mass Transfer Operations, McGraw Hill, p. 333, (1980).
16. Sheldon, R.A. and Kochi, J.K., Metal-Catalyzed Oxidations of Organic Compounds, Academic Press, NY, (1981).
17. Serio, M.A., Malhotra, R., Kroo, E., Deshpande, G.V., Solomon, P.R., "Thermal Stability of Aviation Fuels", Final Report for Contract F33615-88-C-2853, March, 1989.

A Review of Computational Approaches for
Chemically Reacting Flows

R. W. Claus
NASA Lewis Research Center, Cleveland, Ohio

INTRODUCTION

Three-dimensional combustor calculations involve detailed modeling of several important physical processes. Airflow, chemical reactions, fuel sprays, and turbulence are just a few of the physical processes that must be described. Many of these processes occur on both a molecular and a macroscopic scale. To exactly describe these processes numerically, one must resolve these scales on a computational mesh. This is clearly beyond current computational resources. To make the computational task tractable, we introduce modeling assumptions. These modeling assumptions limit the generality of the computational flow code, but it is hoped that the dominant physics remain correctly represented.

Modeling assumptions are only the first limit of generality introduced when developing a combustor flow code. A further limit is introduced by the need to approximate the modeled equations before they are solved numerically. This approximation process can significantly affect the accuracy of a model prediction.

In view of all these factors, a combustor designer cannot be expected to fully embrace a computer model prediction. If a clear distinction between modeling errors and numerical approximation errors cannot be made, then the designer is left with a very unreliable computational tool.

The tremendous growth in computing power, however, has significantly improved our ability to address these issues. Faster computational speeds and larger memories has permitted the development of more complex turbulence/reaction models and the use of finer computational meshes. As a consequence, a new generation of computational tools are becoming available for the design of both high and low speed combustors. This review will examine some recent improvements in combustion models while noting some of the remaining roadblocks.

Discussion

This review will initially focus on the issues being examined in low speed combustion systems, and then will review some of the work being done for high speed applications. This review is not all inclusive but should be representative of the current state-of-the-art used in combustion system design.

Subsonic Combustion

The lack of shock waves and the frequently imposed assumption that acoustic waves can be neglected, significantly reduces the computational burden for subsonic reacting flows. Before examining reaction models, it is instructive to examine how well a few typical flow fields can be numerically predicted.

A number of alternatives exist to solve the fluid flow equations. The main distinguishing characteristic is how turbulence is represented. The most common approach and the least computationally taxing is to either time or Favre average the Navier Stokes equations. Closure for this class of flow codes employs some type of multi-equation turbulence model, the most common being a two-equation model, ref. 1. Figure 1 displays the results of a three-dimensional flow calculation compared to experimental data. The calculations were made using a two-equation turbulence model for two different geometries. Although the flows are highly similar, the numerical results are significantly different. To examine the effect of mesh refinement, the geometry with the least favorable agreement was used in an extensive mesh refinement study. Figure 2 displays the results of a series of progressively finer meshes. Figure 2a indicates that the mean flow field variables show significant improvement with mesh refinement. The same is true for fluctuating flow quantities as seen in figure 2b. While the trend with mesh refinement is encouraging, it is important to keep in mind the fact that this calculation was for a single, three-dimensional jet-in-crossflow, while a complete combustion system contains many jets and other complex flow features. It is impractical to consider using as many as 2 million mesh points for every complex feature of a typical combustor.

Even if one has sufficient mesh resolution, a two-equation turbulence model is inappropriate for many flows. Figure 3 displays a comparison between a calculated turbulence kinetic energy and experimental data for a two-dimensional, bluff-body, flow field, ref. 2. There is a large region in the flow field where there is a significant discrepancy between experiment and calculation. Mesh refinement does not significantly improve the comparison. The disagreement has been conjectured to be due to large scale vortical structures in the flow field. This bluff body type of flow field is sensitive to instabilities that produce vortical structures that can alter the development of the flow.

Whether or not these structures are defined as turbulence, it is clear that for some flows it is important to include these structures in the calculation. There are two computational alternatives to include these structures. The first, and most practical, is a Large Eddy Simulation (LES). Large Eddy Simulations involve the solution of the time-accurate, Navier Stokes equations to directly resolve the large scale structures and some form of a turbulence model is used to represent more "universal" small scale structures. But even for this class of computations, the lim-

itation remains the turbulence closure used to represent the so-called "universal" small scales. Figure 4 displays the results of a Large Eddy Simulation where both the vortical structure resolved in the calculation and the energy imparted by the turbulence model is shown, ref. 3. The large scale vortices resolved in the calculation agree fairly well with experimental data, but the energy in the turbulence model forms in the incorrect locations. Experimental evidence indicates that the turbulence model should form maximums in the braid region of the vortical structure, but the calculations indicate maximums in the core of the vortices. A second, and less practical approach, to resolve large scale structures is Direct Numerical Simulation (DNS). Direct Numerical Simulations resolve all scales of turbulence on a computational mesh and as a consequence this technique is only applicable for low Reynolds number flows. DNS will not be used to calculate real combustor flow fields, but it may be used to develop more appropriate turbulence models. For example, figure 5 displays the results of a Direct Numerical Simulation where several types of perturbations were added to a flow field to augment the amount of product formed, ref. 4. A dashed type in the figure indicates what would happen if just natural noise was used in the flow. Apparently, the amount of product that is formed can be increased by several factors if the proper forms of forcing are used. In an analogous manner Direct Numerical Simulations can be used to test reaction closures, ref. 5.

Supersonic Combustion

Supersonic combustion certainly imposes severe demands on computational analysis. Although the effect of turbulence may be reduced, ref. 6., it does not go away. Shock waves and the need for detailed finite rate chemistry add large demands for additional mesh resolution and long running times.

A flow field that is analogous to the one examined for subsonic flows is the supersonic jet in cross flow. Figure 6 displays the results of a calculation compared with experimental data from ref. 7. The predictions are for a scalar tracing the jet penetration. The contour level that penetrates the furthest should be compared to the data points. The comparison is very good, but it should be noted that these results are sensitive to mesh refinement. Other flow fields where the blowing rate of the jet is changed are not as well predicted.

With the combined requirement to treat finite rate chemistry and turbulence in compressible flows, Probability Density Function (PDF) methods are being developed for high speed flow codes. Some preliminary calculations, using this technique, have shown very promising results for some simple flows. It remains to be seen if an approach that is this computationally difficult can be usefully included into a design process.

Concluding Remarks

The computational approaches that can be used to calculate both subsonic and supersonic reacting flows have been examined. In general, it has been shown that none of these approaches are perfect, but the technology is rapidly developing. The most promising approaches to improved computational accuracy have been illustrated.

References

- [1] Launder, B. E. and Spalding, D.B., "The Numerical Computation of Turbulent Flows," *Computer Methods in Applied Mechanics and Engineering*, 3, 1974, pp. 269-289.
- [2] Claus, R.W., "Modeling Turbulent, Reacting Flow," in *Combustion Fundamentals*, NASA CP 2433, 1985, pp. 31-46.
- [3] Claus, R.W., Huang, P.G. and MacInnes, J.M., "Time-Accurate Simulations of a Shear Layer Forced at a Single Frequency," NASA TM 100836, 1988.
- [4] Claus, R.W., "Response of a Chemically Reacting Shear Layer to Streamwise Vorticity," AIAA paper no. AIAA-89-0978, 1989.
- [5] Riley, J.J. and Metcalfe, R.W., "Direct Simulations of Chemically Reacting Turbulent Mixing Layers," NASA CR-174640, 1984.
- [6] Papamoschou, D., "Experimental Investigation of Heterogeneous Compressible Shear Layers," Ph. D. Thesis 1986.
- [7] Yu, S-T, Tsai, Y-L, Shuen, J-S, "Three-Dimensional Calculation of Supersonic Reacting Flows Using an LU Scheme, AIAA paper no. AIAA-89-0391, 1989.

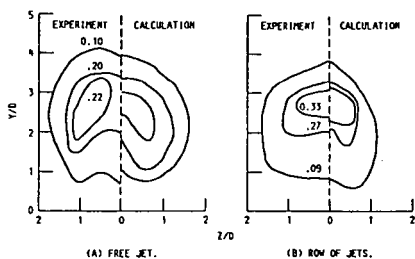


Figure 1. Comparison between experiment and calculation for two parametrically different three-dimensional flow fields.

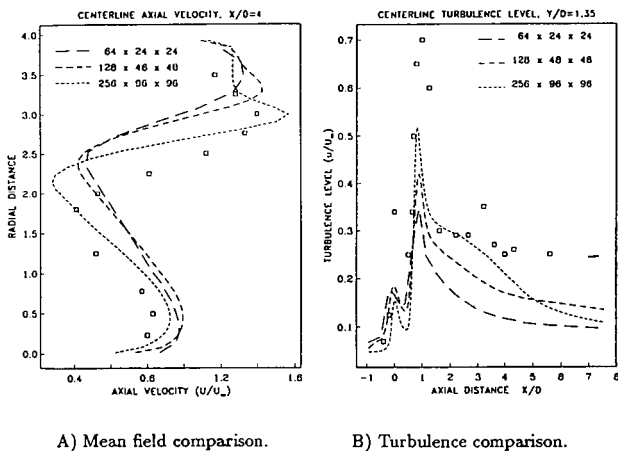


Figure 2. The effect of mesh refinement on a comparison with experimental data for a jet-in-crossflow.

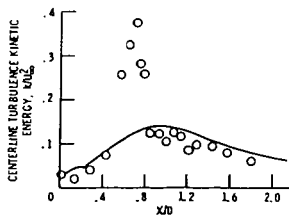
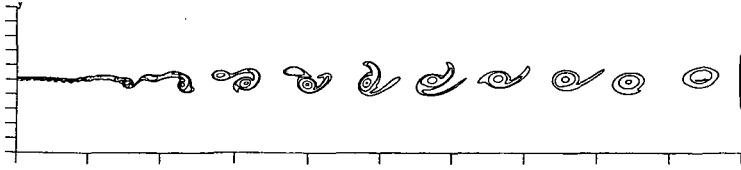


Figure 3. Comparison of a laboratory experiment with numerical prediction for a two-dimensional flow field.



A) Vorticity field.



B) Turbulence kinetic energy.

Figure 4. Results of a Large Eddy Simulation of a forced shear layer.

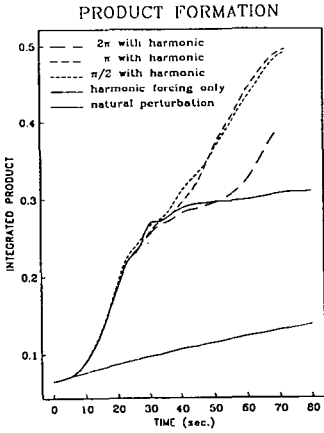


Figure 5. Temporal evolution of the product formed by a perturbed shear layer.

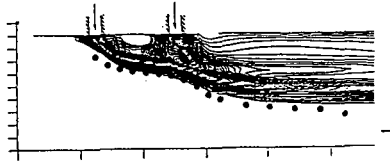


Figure 6. A comparison between predicted and experimental jet penetration in a supersonic flow field.

**THE CALCULATION OF
HIGH-TEMPERATURE REACTION RATE CONSTANTS
USING AB INITIO POTENTIAL ENERGY SURFACES:
EXAMPLES FOR AIR AND HYDROGEN-AIR SYSTEMS**

Richard L. Jaffe
NASA Ames Research Center
Moffett Field, CA 94035

and
Ronald J. Duchovic and Stephen P. Walch
ELORET Institute
Sunnyvale, CA 94087

NASA has always been concerned with the development of new concepts for spacecraft and hypersonic aircraft. Vehicles and propulsion systems currently under investigation[1,2] would use novel combustion systems such as the air-breathing supersonic combustion ramjet engine (SCRAMjet) and fuels such as hydrogen. These vehicles would undergo prolonged operation in the low-density air regime where thermal and chemical equilibrium may not be maintained[3], both in the boundary layer outside the vehicle and inside the combustor. It is also not possible to completely duplicate these flight conditions in ground-based test facilities such as shock tunnels or arc-jets. As a result, extensive computer simulations of the air foil and engine performance are being used in the development and design of these vehicles. In order to properly account for the non-equilibrium effects, detailed chemical models must be incorporated into the computational fluid dynamics (CFD) equations.

One of the tasks undertaken by the Computational Chemistry Branch at NASA Ames Research Center is to provide critically needed chemical and physical data for the CFD models that are being used to simulate the performance of these hypersonic vehicles. In order to reliably predict cross sections and rate constants for the important high-temperature collisional processes we use a three-step approach[4] as outlined below.

First it is necessary to determine an accurate potential energy surface (PES) for the reaction system as described in a previous paper of this symposium by Walch *et al.* The PES gives a measure of the net interatomic forces between the colliding atomic and molecular species. It is usually determined, for a small set of selected atomic geometries, as discrete energies resulting from large-scale *ab initio* quantum chemical calculations. Often these data points are clustered around the saddle point or along the minimum energy path (MEP) connecting reactant and product geometries. The energy difference between the reactants and saddle point is generally comparable to the experimental activation energy.

Second, an interpolating function must be developed to provide values of the interaction energy at any atomic geometry required by the specific reaction dynam-

ics model being used. The determination of the interpolating function is not an easy task and depends, to a certain extent, on the amount of *ab initio* data available as well as the nature of the system studied. In the present study, we have used the valence-bond derived LEPS[5] and the Sorbie-Murrell (SM)[6] approach to represent global PES and piecewise polynomial fits to represent regions around the saddle point or along the MEP. In the LEPS method, electronically excited diatomic fragment potential energy curves are treated as adjustable fitting functions to control the topography of the PES. Their parameters are adjusted to reproduce the saddle point geometry and height, if it is known, and/or some experimental measure of the reaction dynamics such as a product scattering angle or product internal state distribution. The LEPS method is generally satisfactory for simple atom-diatom exchange reactions occurring on purely repulsive potential energy surfaces. However, if a collinear approach between reactants is not favored, or if intermediate complex formation is possible, the PES cannot usually be represented by the LEPS method. A more promising method for general systems is the SM method, which is based on the sum of an arbitrary series of terms describing all possible 2-body to *n*-body interactions. The increased flexibility of treating each term separately is a powerful feature of the method.

The final step in the procedure is the calculation of reaction dynamics and kinetics. In general, the reaction dynamics is treated using classical mechanics[7] which should not cause a significant error, especially for collisions well above threshold. Furthermore, in spite of the fact that systems containing hydrogen atoms may have important quantum effects, such as tunneling, we expect that the calculated rate constants should still be accurate at high temperatures. We also use statistical models such as canonical variational transition state theory (CVT)[8] to calculate rate constants. The statistical models allow for the inclusion of quantization of energy levels and corrections for tunneling in an approximate manner.

The classical trajectory method has been a standard approach for the calculation of the dynamics and kinetics of gas phase collisions of small molecules for more than 30 years. The calculations consist of integrating the classical equations of motion for an isolated collision between the reactant species. The propagation of these equations in time for a set of initial coordinates and momenta is called the calculation of a single trajectory and corresponds to the motion of the colliding species over a time period of ≈ 1 ps. Through the application of appropriate random sampling techniques, the behavior of an ensemble of molecules with a collision frequency of 10^{20} s^{-1} can be simulated by on the order of 10^4 trajectories.

Statistical models of chemical kinetics such as transition state theory have been in existence for more than 50 years. However, for the last 10 years, Truhlar and coworkers have systematized numerous models and concepts under the label of variational transition state theories (VTST)[8]. In this model, the optimal transition state is chosen to be the location along the intrinsic reaction path for which the free energy is minimized. Some versions of VTST use quantized anharmonic descriptions

of the transition state energy levels and include tunneling corrections. The VTST model has been thoroughly tested for elementary gas phase reactions and shown to be in agreement with experimental data and the results of classical and quantum scattering calculations.

In this presentation we first demonstrate the computational methods and give details of the calculations using the air exchange reaction



as an example. Walch and Jaffe[9] have completed *ab initio* calculations for this system of the two low-lying PES that connect the ground electronic states of reactants and products. These are the $^2A'$ and $^4A'$ surfaces with saddle point energies of 10.2 and 18.0 kcal/mol, respectively, referenced to the minimum in the $N + O_2$ asymptote (it was estimated that the calculated $^2A'$ saddle point energy is too high by ≈ 2 -3 kcal/mol). The MEP for both surfaces favored a 110° approach of the reactants. An additional complicating factor for the $^2A'$ PES is the presence of a deep potential well corresponding to the ground electronic state of the NO_2 molecule.

Fits to both $N-O-O$ surfaces were obtained using a modification[10] of the LEPS approach: an additional angle dependent term was added to shift the favored angle of approach from collinear to 110° . The resulting potential energy function provided a satisfactory representation of the PES for the $^4A'$ surface where only a small amount of *ab initio* data was available. It was not, however, satisfactory for the $^2A'$ PES. For that case, a more elaborate formulation based on the SM method has been developed[11]. As of this writing, the improved $N-O-O$ doublet potential energy function has not yet been used for trajectory calculations.

We have computed thermal rate constants for the $N + O_2$ reaction based on ensembles of 5000 trajectories at each temperature. The results shown in Figure 1 are the combined rate constants for exchange and dissociation. The rate constants for reaction occurring on the $^2A'$ and $^4A'$ surfaces have been combined with the proper degeneracy factors of 1/6 and 1/3, respectively. Below 2000 K reaction on the quartet surface makes little contribution to the overall rate constant because of the higher energy barrier. However, the larger degeneracy factor causes this process to become dominant at temperatures greater than 3000 K. Dissociation does not contribute significantly at temperatures below 5000 K. As can be seen from the figure, the agreement between the calculated and measured rate constants[12,13] is quite good. Calculations of VTST rate constants for this reaction are in progress.

In addition, statistical calculations of the rate constants for the reactions:



and



will be presented. The former is an important chain branching step in H_2/O_2 combustion. We have computed high-pressure limiting rate constants for HO_2

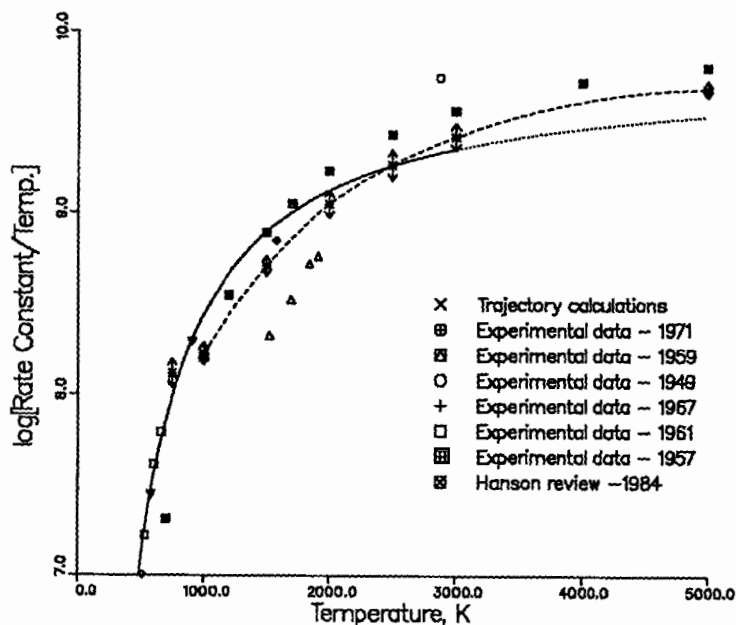


Figure 3. A comparison of the theoretical and experimental rate constants for $N + O_2 \rightarrow NO + O$.

formation using the MEP from *ab initio* PES calculations[14,15] and will also report VTST calculations for the exchange reaction. These results will be discussed in terms of the discrepancies in the measured high-temperature rate constants. The latter reaction has been suggested as the initiation step in the $H_2 + O_2$ reaction mechanism. However, no experimental data exist for this process.

REFERENCES:

1. "Pioneering the Space Frontier", Report of the National Commission on Space, (Bantam Books, New York, 1986).
2. G. Y. Anderson, "An Outlook on Hypersonic Flight", AIAA Paper 87-2074, AIAA/SAE/ASME/ASME 23rd Joint Propulsion Conference, San Diego, CA, June 1987.
3. D. M. Cooper, R. L. Jaffe and J. O. Arnold, *J. Spacecraft and Rockets* **22**, 60 (1985).
4. R. L. Jaffe, M. D. Pattengill, and D. W. Schwenke, to be published in the proceedings of the NATO Advanced Research Workshop *Supercomputer Algorithms on Reactivity, Dynamics and Kinetics of Small Molecules*, Colambella di Perugia, Italy, August 30-September 3, 1989, edited by A. Lagana (D. Reidel, Dordrecht, Holland).

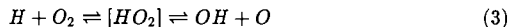
5. J. C. Polanyi and J. L. Schreiber, "The dynamics of Bimolecular Reactions," in *Physical Chemistry - An Advanced Treatise, Vol. VI, Kinetics of Gas Reactions*, edited by H. Eyring, W. Jost and D. Henderson (Academic Press, New York, 1974), p. 383.
6. K. S. Sorbie and J. N. Murrell, *Mol. Phys.* **29**, 1387 (1975).
7. D. G. Truhlar and J. T. Muckerman, in "Atom-Molecule Collision Theory", ed. by R. B. Bernstein (Plenum Press, New York, 1979), chap. 16.
8. D. G. Truhlar, A. D. Isaacson, and B. C. Garrett, "Generalized Transition State Theory," in *Theory of Chemical Reaction Dynamics*, edited by M. Baer (CRC Press, Boca raton, FL, 1985), Vol 4, pp. 65-137.
9. S. P. Walch and R. L. Jaffe, *J. Chem. Phys.* **86**, 6946 (1987).
10. M. D. Pattengill, R. N. Zare and R. L. Jaffe, *J. Phys. Chem.* **91**, 5489 (1987).
11. R. L. Jaffe, M. D. Pattengill, T. Halicioglu, and S. P. Walch, manuscript in preparation.
12. D. L. Baulch, D. D. Drysdale, and D. G. Horne, "Evaluated Kinetic Data for High Temperature Reactions, Vol. II Homogeneous Gas Phase Reactions of the $H_2 - N_2 - O_2$ System" (Butterworth, London, 1973).
13. R. K. Hanson and S. Salimian, "Survey of Rate Constants in the $N/H/O$ System", in *Combustion Chemistry*, edited by W. C. Gardiner, Jr., (Springer-Verlag, New York, 1984), p. 361.
14. S. P. Walch, C. M. Rohlfling, C. F. Melius, and C. W. Bauschlicher, *J. Chem. Phys.* **88**, 6273 (1988).
15. R. J. Duchovic and S. P. Walch, unpublished results.

AB INITIO POTENTIAL ENERGY SURFACES FOR CHEMICAL REACTIONS

Stephen P. Walch[†] and Ronald J. Duchovic[†]
Eloret Institute, Sunnyvale, CA 94087
and
Celeste McMichael Rohlffing
Sandia National Laboratories, Livermore, CA 94551-0969

NASA is currently pursuing programs of interplanetary exploration and manned flight which require a detailed understanding of the physics and chemistry occurring in hypersonic flow fields. Specifically, research efforts have focused on the bow shock layers which form in front of hypersonic vehicles and on the combustion processes of the supersonic combustion ramjet (SCRAMjet) which will power a future generation hypersonic aircraft. The chemistry of the hypersonic flow problem is particularly complex because the reactant species are expected to have non-equilibrium rovibrational distributions [1] under conditions of temperature, pressure, and flow rates which make the experimental measurement of reaction rates extremely difficult. In the case of the SCRAMjet, the short residence times make finite rate chemistry critical to the design of the engine. Consequently, the calculation of reaction rates from first principles has become an important component of the NASA research program.

Ab initio calculations designed to investigate the potential energy surfaces (PESs) of a number of reactions involving hydrogen, oxygen, and nitrogen have now been completed. In particular, the following reactions will be discussed:



Reaction (1) is an important process in the high temperature chemistry of the bow shock layer created by the passage of hypersonic vehicles through atmospheres whose components include nitrogen and oxygen. Reaction (2) is an initiation step while

[†] Mailing address: NASA Ames Research Center, Moffett Field, CA, 94035

reaction (3) represents a critical chain-branching step in the H_2/O_2 combustion process. Reaction (4) is a possible two-step mechanism (chaperon mechanism) for the termolecular recombination of H atoms in the presence of N_2 ($\text{H} + \text{H} + \text{N}_2 \rightarrow \text{H}_2 + \text{N}_2$).

The calculation of reaction rates from first principles relies on both *ab initio* electronic structure theory and an appropriate dynamical theory. The first step requires the calculation of accurate approximations to the potential energy for a limited number of selected geometrical arrangements of the atoms involved in the reaction. One of several available dynamical techniques is then chosen to calculate the rate of reaction. The choice of technique is dictated both by the nature of the reaction under investigation and by the completeness of the calculated *ab initio* PES. If the calculated data is limited to the stationary points of the PES, a local representation of the PES in the neighborhood of these stationary points is determined, allowing the use of only the most elementary statistical theories to calculate the rate of reaction. If there is sufficient information to characterize accurately the minimum energy path (MEP) of the reaction, then either reaction path Hamiltonian methods or more sophisticated statistical methods can be employed in the rate calculation. Finally, if the *ab initio* data is sufficiently complete to permit the development of a global representation of the PES, then either classical trajectory or quantum scattering methods can be utilized to calculate the rate of reaction. Jaffe *et al.* will discuss the second stage of this computational procedure in a separate paper to be presented in these proceedings.

While the details of the *ab initio* computations are reported in Ref. 2-5, a brief summary of the methodology is given here. The zero-order wave function is a complete active space self-consistent field (CASSCF) wave function. For a given choice of active orbitals, every possible configuration which can be constructed by distributing the active electrons among these active orbitals is included in the wave function. The orbitals and mixing coefficients of the configuration interaction (CI) expansion are then optimized. The orbitals themselves are expanded in a finite set of atom-centered basis functions. While a basis set constructed from a segmented contraction of primitive functions was used in the study of reaction (1), the remaining calculations discussed here utilized basis functions derived from the natural orbitals of CI calculations performed on the atoms (for H atom, these calculations were performed on the H_2 molecule). The CASSCF calculation is then followed by a multireference contracted CI calculation (CCI) which allows single and double excitations from the set of reference configurations (the set of configurations which are most important in the CASSCF wave function).

Walch and Jaffe [2] have completed *ab initio* calculations for the $^2\text{A}'$ and $^4\text{A}'$ PESs of reaction (1). These calculations indicated that the $^2\text{A}'$ surface has an early barrier of 10.2 kcal/mol, while the $^4\text{A}'$ surface exhibits a barrier of 18.0 kcal/mol

(Note that none of the energies discussed in this paper include corrections for zero-point energy.). Initial global representations of these two surfaces (modified LEPS potential functions) have been constructed and used in a preliminary examination [6] of the kinetics of this reaction. Further, a more accurate functional representation of the $^2A'$ surface has been completed recently [7] and will be used in future studies supporting the development of aeroassisted orbital transfer vehicles (AOTVs).

An earlier *ab initio* study [8] of reaction (2) identified a saddle point geometry which resembles the H + HO₂ reactant configuration and a barrier of 6.3 kcal/mol. A conventional transition state theory calculation (including a Wigner tunneling correction) which treated the barrier height as an adjustable parameter required a barrier of ≈ 2.7 kcal/mol in order to reproduce the reaction rate measured experimentally at room temperature. The present *ab initio* calculations, using a larger basis set, estimate the barrier height to be 3.7 kcal/mol.

The MEP for H atom addition to O₂ is very similar to that found in an earlier study [9] of the same reaction. At large H-O₂ separations, the H atom initially approaches the O₂ molecule at an HOO angle of $\approx 119^\circ$. This angle gradually decreases to $\approx 104^\circ$, while r_{OO} gradually increases as the HO bond forms. These calculations (at the CCI level of theory) exhibit a barrier to H atom addition of ≈ 0.4 kcal/mol.

Two additional regions of the PES for reaction (3) which have not been studied previously were investigated in the current work. The first is the region which governs the exchange of the H atom between the two oxygen atoms. The saddle point for this process is found to be ≈ 13 kcal/mol below the H + O₂ asymptote, making this region of the PES accessible during the formation of [HO₂] from both H + O₂ and OH + O. The second region is the OH + O channel which is complicated by the competition between a long-range classical electrostatic force (a dipole-quadrupole interaction) which favors a linear OH-O geometry, and the short-range chemical bonding interaction which favors a bent [HO₂] species.

The HN₂ species (reaction (4a)) is found to lie ≈ 3.0 kcal/mol above the H + N₂ asymptote with a barrier of ≈ 12 kcal/mol between HN₂ and H + N₂. This calculated potential well contains six quasibound (harmonic) vibrational energy levels. A conventional transition state theory calculation which approximated tunneling with a one-dimensional Eckart model estimates the lifetime of HN₂ in the lowest vibrational level to be less than 6×10^{-9} s. This result is consistent with a recent experimental [10] estimate of less than 5×10^{-7} s for this lifetime.

A plot of the potential energy for reaction (4b) is shown in the figure. There are four pathways, three of which lead to stable N₂H₂ species, and a fourth which leads to H₂ + N₂. It is expected that reaction (4b) will lead to stabilized H₂ since the excess energy of the reactants can be dissipated either as relative translational

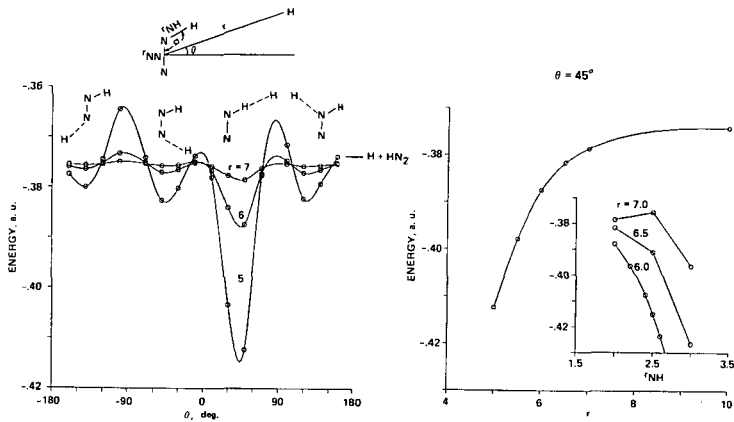


Figure 1. Plot of the potential energy for reaction (4b). In the left half of the figure the HN_2 geometry is held fixed near its optimal geometry and the H to N_2 center of mass distance, r , as well as the angle, θ , are varied. In the right half of the figure, θ is held fixed at 45° while r and r_{NH} are varied.

energy or rovibrational energy in the products. Because there is no potential energy barrier to the formation of $\text{H}_2 + \text{N}_2$, it might be expected that the production of H_2 will occur at or near the gas kinetic collision frequency. Estimates of the formation and dissociation rates of HN_2 combined with an estimate of the rate for reaction (4b) would yield an overall termolecular rate (chaperon mechanism) for the recombination of H atoms in the presence of N_2 .

REFERENCES

1. E. E. Whiting, J. O. Arnold, W. A. Page, and R. M. Reynolds, *J. Quant. Spectrosc. Radiat. Transfer* **13**, 837(1973).
2. S. P. Walch and R. L. Jaffe, *J. Chem. Phys.* **86**, 6946(1987).
3. S. P. Walch, C. M. Rohlffing, C. F. Melius, and C. W. Bauschlicher, *J. Chem.*

- Phys. **88**, 6273(1988).
4. S. P. Walch, R. J. Duchovic, and C. M. Rohlring, *J. Chem. Phys.* **90**, 3230(1989).
 5. S. P. Walch, *J. Chem. Phys.*, in press.
 6. R. L. Jaffe, M. D. Pattengill, and D. W. Schwenke, to be published in the proceedings of the NATO Advanced Research Workshop *Supercomputer Algorithms on Reactivity, Dynamics, and Kinetics of Small Molecules*, Colombella di Perugia, Italy, August 30-September 3, 1989, D. Reidel, Dordrecht, Holland.
 7. R. L. Jaffe, M. D. Pattengill, T. Halicioglu, and S. P. Walch, manuscript in preparation.
 8. L. B. Harding, private communication.
 9. T. H. Dunning, Jr., S. P. Walch, and M. M. Goodgame, *J. Chem. Phys.* **74**, 3482(1981).
 10. S. F. Selgren, P. W. McLoughlin, G. I. Gellene, *J. Chem. Phys.* **90**, 1624(1989).

CRITICAL REACTION RATES IN HYPERSONIC COMBUSTION CHEMISTRY

Richard C. Oldenborg, David M. Harradine, Gary W. Loge,
John L. Lyman, Garry L. Schott, and Kenneth R. Winn

Los Alamos National Laboratory
Los Alamos, New Mexico 87545

INTRODUCTION:

High Mach number flight requires that the scramjet propulsion system operate at a relatively low static inlet pressure and a high inlet temperature. These two constraints can lead to extremely high temperatures in the combustor, yielding high densities of radical species and correspondingly poor chemical combustion efficiency. As the temperature drops in the nozzle expansion, recombination of these excess radicals can produce more product species, higher heat yield, and potentially more thrust. The extent to which the chemical efficiency can be enhanced in the nozzle expansion depends directly on the rate of the radical recombination reactions.

Radical recombination reactions rely on collisions to stabilize products, and consequently the rates of these reactions are, in general, pressure dependent. The low pressures inherent in high Mach number, high altitude flight can, therefore, slow these reaction rates significantly, relative to their rates in more conventional propulsion systems. This slowing of the chemistry is further compounded because high Mach number flight also implies high internal velocities that result in very short residence times (millisecond time range) in a hypersonic engine. Consequently, the finite rates of these chemical reactions may be a limiting factor in the extraction of the available chemical energy. A comprehensive assessment of the important chemical processes and an experimental validation of the critical rate parameters is therefore required if accurate predictions of scramjet performance are to be obtained.

IDENTIFICATION OF CRITICAL REACTIONS:

A chemical kinetics computer simulation code has been employed for modeling the hydrogen/air combustion in a basic hypersonic ramjet engine design. The code

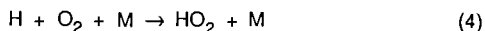
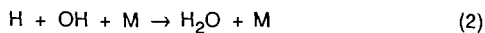
models the kinetics and thermomechanics of premixed, quasi-one dimensional, time-steady streamline segments. Details of the calculations and the reaction rate constants employed are presented elsewhere [1]. The code is far simpler than conventional CFD codes, and does not consider the effects of mixing, conduction, convection, or diffusion. Our motivation is not to accurately predict scramjet performance, but to assess the role of finite-rate chemistry in the combustion process and to identify key rate-limiting steps in the combustion process.

Using this code, comparisons were made, for a variety of engine designs and flight conditions, between calculations involving finite-rate chemistry and those in which equilibrium conditions are maintained. In particular, radical densities and the energy yield, i.e., the fraction of the maximum possible heat of combustion achieved, were examined. From these comparisons, we find that the use of finite-rate chemistry models in the combustor section has only a minimal effect on the predicted performance. In contrast, very large differences are observed in the nozzle expansion, driven by the rapid drop in pressure and temperature. The finite-rate chemistry model predicts significantly higher radical concentrations at the nozzle exit, with a corresponding decrease in energy yield.

A sensitivity analysis of the chemical reaction model was conducted to identify which reactions are the key rate-limiting steps in the heat release mechanism during the nozzle expansion. Most of the bimolecular reactions, such as



were found to be very fast under typical scramjet operating conditions and tend to reach a partial equilibrium. Consequently, the exact magnitude of the bimolecular reaction rate constants that are involved should have little impact on the overall chemistry. In contrast, four termolecular radical recombination reactions were found to be particularly rate- and, therefore, performance-limiting. These critical limiting reactions are:





The important collision partners, collectively denoted as M in the above expressions, are H₂O, N₂, H₂, and possible H-atoms under typical hypersonic combustion conditions. The relative importance of these four reactions varies with equivalence ratio. All tend to be significant under stoichiometric conditions. As might be expected, the importance of reaction (3) decreases in fuel lean conditions, while reactions (4) and (5) decrease in fuel rich conditions.

The exact rate constants for these selected reactions that are used in the simulations can dramatically affect predicted combustion efficiency and engine performance. It is therefore of critical importance that the rate constants for these reactions be well determined if accurate predictions of scramjet performance are to be obtained.

The accuracy to which the rate constants for these processes are presently known was examined. Figure 1 summarizes the published data acquired over the past half century for reaction (2), where M = H₂O. For references to the original studies from which these data were obtained, refer to the Leeds compilation [2]. The data in figure 1 fall into two groups, high temperature measurements around 2000K from flame and shock tube experiments, and room temperature data from flash photolysis experiments. The span in the rate constant data at either temperature is nearly two orders-of-magnitude. The solid line in the figure is the recommended value of Baulch et al. [2], but clearly the large spread in the data on which this recommendation is based reveals the unacceptably large uncertainties inherent in this value, as noted in the original compilation. Examination of the data for reaction (2) with other collision partners, M, as well as the data for reactions (3), (4), and (5) show similar uncertainties. The critical importance of these recombination reactions to nozzle performance, combined with the large unacceptable scatter in the literature data, indicate that these reactions are prime candidates for experimental study.

EXPERIMENTAL MEASUREMENTS:

The rate constants for reactions identified through the modeling simulations as critical for good scramjet performance are being experimentally determined using the laser photolysis / laser-induced fluorescence (LP/LIF) relaxation kinetics technique. In this technique, water vapor, containing various added amounts of hydrogen, oxygen, and/or nitrogen, is equilibrated at temperatures extending from room temperature to 1800K (3200R) and at total pressures in the range 7 - 30 psia. This equilibrium mixture will be perturbed essentially instantaneously using excimer laser photolysis so

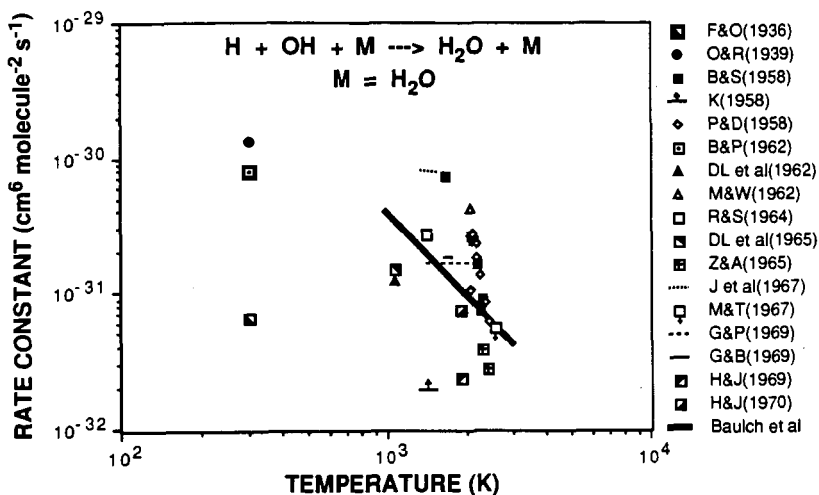


Figure 1. Summary of published rate constant data for H + OH + M reaction.

as to increase the concentrations of the OH radicals and H atoms by



The absolute densities of the photolytically introduced radicals can be determined from the laser fluence and an independently determined photodissociation cross section for water vapor. Laser-induced fluorescence is then used to monitor the subsequent time histories of the OH and/or H as they return to their equilibrium concentrations. The time required for the chemical system to return to equilibrium, i.e., the relaxation time, is measured and compared to predictions of the chemical kinetic modeling code under identical conditions. Since this technique simultaneously evaluates the entire relaxation mechanism, we can be assured that all key reactions are addressed in the experiment and that a self-consistent set of rate constants can be obtained.

Before beginning the recombination rate constant measurements, direct measure-

ments of the rate constant for the bimolecular reaction



were completed in the temperature range 800-1550K. The OH is removed by this reaction as the partial equilibration of the OH and H-atom densities is attained. Analysis of the fast OH removal rates as a function of added hydrogen yields the rate constant for the above reaction.

The rate constant for this reaction has been well determined in a number of previous studies by other workers and was recently reexamined by Michael and Sutherland [3]. They combined their shock tube data with those of Frank and Just and the flash photolysis data of Tully, Ravishankara, and co-workers, and derived the expression:

$$k = 3.59 \times 10^{-16} T^{1.51} \exp[-1726 / T] \text{ cm}^3\text{molecule}^{-1}\text{s}^{-1},$$

which is applicable in the temperature range 250-2581 K. Our recent measurements bridge the gap between the shock tube data (1246-2581 K) and the flash photolysis data (250-1050 K) and are in very good agreement with these previous data sets in the overlap region. Our data points lie slightly above the fit expression recommended by Michael and Sutherland. We combined our data with the three data sets they used and the recently reported data [4] of Davidson, Chang, and Hanson, to derive a new expression for the rate constant:

$$k = 3.56 \times 10^{-16} T^{1.52} \exp[-1736 / T] \text{ cm}^3\text{molecule}^{-1}\text{s}^{-1}.$$

The constants in this expression are nearly identical to those in the Michael and Sutherland expression. However, the rate constants calculated with this new expression are a few percent higher, averaged over the entire temperature range. Figure 2 shows an Arrhenius plot of our recently obtained data (LANL) along with some of the other data values obtained from published papers and used in determining the fit expression. The fit line shown in the figure is based on our recommended expression. These results are presently being prepared for publication.

The purpose of these measurements was to validate the kinetic measurement techniques employed in these experiments by reevaluating a well known rate constant, in preparation for our recombination rate constant measurements. Having achieved this objective, our studies have begun on the recombination reactions.

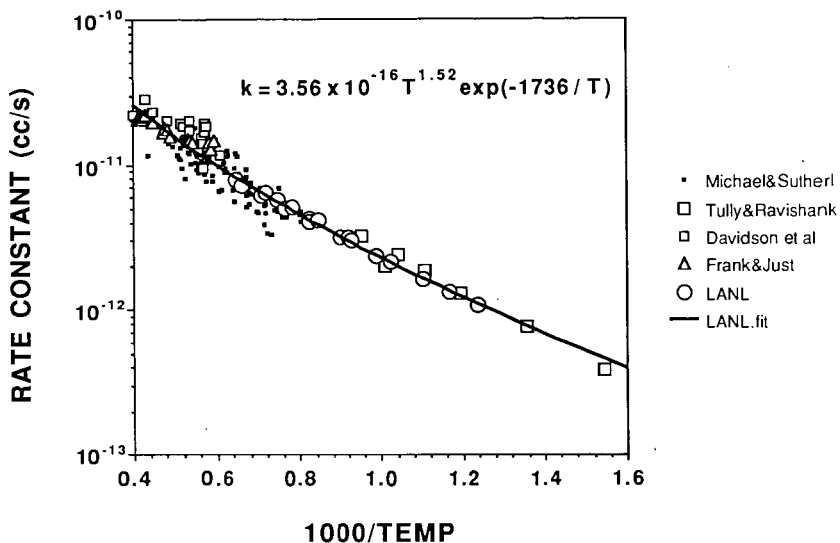


Figure 2. Arrhenius plot of rate constant data for $\text{OH} + \text{H}_2 \rightarrow \text{H} + \text{H}_2\text{O}$ reaction.

Preliminary rate constant values for recombination reactions (2) and (3) have now been obtained at a single temperature (1223 K). However, the uncertainty of these measurements is at present unacceptably large. Relaxation rate measurements at this temperature for additional gas compositions are in progress. Variation of the gas composition allows different reactions to dominate the chemistry, and consequently this additional data should improve the precision of these rate constant determinations. Over the next few months, the temperature range of these measurements will be extended to the limits of our present high temperature cell (300 - 1800 K). The wide temperature range of these experiments (note Fig. 1) should allow accurate extrapolations of these new rate constants into temperature regimes of relevance for hypersonic combustion. The status of these measurements will be discussed in the presentation.

REFERENCES:

1. D. Harradine, J. Lyman, R. Oldenborg, G. Schott, and H. Watanabe, "Hydrogen/Air Combustion Calculations: The Chemical Basis of Efficiency in Hypersonic Flows," AIAA Journal (submitted, 1989).
2. D. L. Baulch, D. D. Drysdale, D. G. Horne, and A. C. Lloyd, Evaluated Kinetic Data for High Temperature Reactions, Vol. I (CRC Press, 1972).
3. J. V. Michael and J. W. Sutherland, J. Phys. Chem., 92, 3853 (1988).
4. D. F. Davidson, A. Y. Chang, and R. K. Hanson, 22nd Symposium (International) on Combustion, in press (The Combustion Institute, 1988).

HOMOGENEOUS CATALYSTS IN HYPERSONIC COMBUSTION

David M. Harradine, John L. Lyman, Richard C. Oldenborg,
Russell T. Pack, and Garry L. Schott

Los Alamos National Laboratory
Los Alamos, NM 87545

INTRODUCTION

Density and residence time both become unfavorably small for efficient combustion of hydrogen fuel in ramjet propulsion in air at high altitude and hypersonic speed. Raising the density and increasing the transit time of the air through the engine necessitates stronger contraction of the airflow area. This enhances the kinetic and thermodynamic tendency of H_2O to form completely, accompanied only by N_2 and any excess H_2 (or O_2). The by-products to be avoided are the energetically expensive fragment species H and/or O atoms and OH radicals, and residual ($2H_2$ plus O_2). However, excessive area contraction raises air temperature and consequent combustion-product temperature by adiabatic compression. This counteracts and ultimately overwhelms the thermodynamic benefit by which higher density favors the triatomic product, H_2O , over its monatomic and diatomic alternatives.

For static pressures in the neighborhood of 1 atm ($\times/+2.5$), static temperature must be kept or brought below ca. 2400 K for acceptable stability of H_2O . In contrast, temperatures exceeding ca. 3200 K at these static pressures actually give net endothermic pyrolysis of H_2 and O_2 , with more atoms than H_2O . Some relief from these limitations on efficient use of low-density air as an oxidant may be realized by expenditure of excess, initially cold fuel whose specific heat protects stability of H_2O and whose ejected mass contributes to thrust.

Another measure, whose requisite chemistry we address here, is to extract propulsive work from the combustion products early in the expansion. The objective is to lower the static temperature of the combustion stream enough for H₂O to become adequately stable before the exhaust flow is massively expanded and its composition "frozen." Prospective success of this measure in an acceptable expansion length is limited by the kinetics of the three-body "recombination" mechanism by which the composition of combustion products can shift exothermically.

We proceed to address this mechanism and its kinetics, and then examine prospects for enhancing its rate by homogeneous catalysts.

UNCATALYZED RECOMBINATION

Recombination Mechanism

The most facile steps by which net recombination is understood to occur among the fragments of H₂O are:



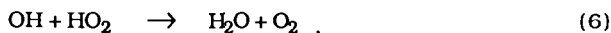
and the sequence



followed by

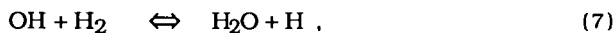


or



The respective exothermicities of steps (1) through (3), expressed as $-\Delta H$ in kcal/mole at zero Kelvin and rounded to the nearest whole number, are: 103, 118, and 101. The corresponding values [1] for steps (4) through (6) are: 49, 54, and 69. The net effects of the (4),(5) and (4),(6) sequences are indistinguishable from (1) and (2), respectively. For modeling, we use a more complete mechanism that includes alternate product channels of step (5) and a step analogous to (6) in which O-atom replaces OH. To set the stage here for the role of catalysts, we proceed without these other steps.

In compositions that are more or less hydrogen-rich, steps (1) and (2) contribute in parallel, in proportions governed by the H/OH ratio and the individual rate coefficients for each step with H_2O , N_2 , H_2 , and even atomic H as third bodies, collectively denoted M. The proportions of the products of steps (1) and (2) are subject to readjustment, with concomitant adjustment of the H/OH ratio. This occurs directly by the bimolecular step



whose exothermicity in the forward direction, as above, is only +15 kcal/mole, and whose forward and reverse rates are both large and become nearly equal. Both (1) and (2) are kinetically second order in the energetic fragments and so both rates diminish quadratically as net recombination is accomplished at fixed density, or as density is diminished by expansion. Up to ca. 2400 K at the densities for which their rates are significant, these steps are substantially irreversible, and their rate coefficients diminish only mildly with increasing temperature.

In stoichiometric and fuel-lean compositions, step (3) and the complex paths formed by steps (4), (5), and (6) are comparatively important, and step (1) not so. The reaction-order and irreversibility characteristics of step (3) are similar to those of steps (1) and (2)

discussed above. The thermochemistry of HO_2 makes reversibility of step (4) a serious complication. Within the (4) - (5)/(6) sequences, step (4) is rate-limiting at high fragment fractions and recombination is first-order in O_2 and H-atom populations. Although excess O_2 is not consumed in proportion to the fragments, progressive recombination diminishes the H-atom population nonlinearly. Reversible step (4) becomes equilibrated and step (6) becomes rate-limiting. And the net recombination rate by the (4)-(6) sequence becomes seriously diminished as temperature is raised above ca. 2000 K, leaving step (3) to become the dominant path near 2500 K in fuel-lean compositions and step (2) in near-stoichiometric compositions.

Hypersonic Flow Simulation

Earlier we [2] have modeled numerically the kinetics and thermomechanics of premixed, quasi-one dimensional, time-steady streamline segments that simulate supersonic H_2 /air combustion in a hypersonic ramjet. Of concern was the chemical basis of combustion efficiency. An undocumented Los Alamos code for finite-rate kinetics and thermochemistry, adapted to this application, was used.

Coupled engine/nozzle flow was simulated for a hypothetical vehicle flying at Mach 15 in air at 1.3×10^5 ft above the earth as a representative case. Stoichiometrically metered gaseous H_2 fuel from a lower temperature source was taken as mixed instantaneously with ram-compressed air at the initial station [3]. Static temperature and pressure of the mixed stream were 1463 K and 447 torr (59.5 kPa; 8.64 psia). Resulting internal axial stream velocity was 4.34×10^3 m/s.

For this base case, computed finite-rate reaction was followed through a 1-m long, constant-area combustor. Following ignition, near-equilibrium composition was reached at 2932 K, with 58% of the ideal combustion energy realized. Fragment species harbored the remaining 42%.

Next, expansion of the flow area beyond this 1-m station was modeled to an area sixteen times the combustor area over 1.5 m of further flow. Effects of selected area vs distance profiles were compared.

Computed static temperatures dropped from near 3000 K to near 1000 K. Computed composition began to shift toward a more complete energy-yield condition, but froze with only modest fractions of the remaining 42% realized.

This model scenario formed the base case for our present numerical examination of effects of added catalyst types in the early expansion.

CATALYZED RECOMBINATION

As potential catalysts for recombination, we may consider two classes:

- (a) Substances that catalyze steps (1)-(4) as third bodies, M, with large rate coefficients; and
- (b) Substances that introduce parallel paths analogous to the HO₂ sequence, (4)-(5)/(6), with such thermochemistry that, like O₂, they are regenerated and not irreversibly consumed.

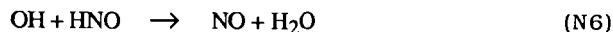
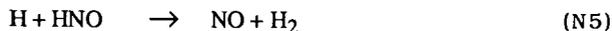
Such catalytic substances can enhance the energy recovery through recombination early in the expansion of combustion products in which ideal combustion is stoichiometrically incomplete owing to too high a temperature for the combustion-stream pressure. They can do so profitably if, in the time of such early expansion, they enable a greater yield of chemical energy and increment of streamline thrust to be achieved than could alternatively be achieved from the combined influences of more complete equilibrium combustion and uncatalyzed early recombination realized from addition of a like mass of excess fuel or "inert" thermal ballast to the combustion flow.

As prospective catalysts we select representative substances from those volatile materials that are known to inhibit flames. These are recognized by their qualitative consequences of lower flame speeds in gaseous systems that include them as additives, and/or wider minimum channel dimensions for flame propagation. Their mode of

action is generally associated with diminished radical populations in the ignition phase of combustion, where radicals (including the atomic species H and O) function as carriers in chain-reaction sequences. Paradoxically, the same agents and recombination mechanisms serve to promote the completion of combustion from an intermediate composition in which ignition coupled with high temperature have produced a surplus of "intermediate" fragments. Since experience teaches that reactions (1)–(4) have almost their largest rate coefficients with H₂O as the third body as with any known species, the flame-inhibiting catalysts we are led to consider come from class (b) above. Two chemical types of these catalysts are distinguished: (i) nonmetals, either as atoms or low-valence oxides, and (ii) molecular metal oxides.

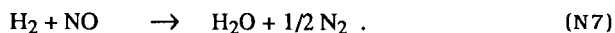
Nonmetal Oxide Catalyst

Nitric oxide, NO, is a prototype catalytic substrate to which H-atoms and also O-atoms and OH radicals each combine in a process analogous to step (4), and will be abstracted in steps analogous to (5)/(6). In each case the bond formed in the three-body step is analogous in strength to the bonds in the HO₂ from step (4). Thus, subsequent abstraction by a second atom or OH radical to form a 100–118 kcal/mole bond is exothermic, in the pattern of steps (5)/(6), and NO is liberated to complete a homogeneous catalytic cycle. The prototype steps for fuel-rich hydrogen-air recombination are:



The full set of steps used in modeling, and their rate coefficients, are conveniently surveyed elsewhere [4].

NO is not stable against atmospheric oxidation or physiologically benign enough to be a useful flame-retarding agent in room-temperature fire protection applications. Its role as a (generally undesirable) by-product of air-based combustion is well studied, however. Its presence in hypersonic propulsion streams is neither wholly avoidable nor dependent upon nonfuel material being carried in the vehicle for addition to the flow. Moreover, the behavior of NO as a recombination catalyst was directly studied early on [5,6] in postflame gases from premixed, fuel-rich, atmospheric pressure $H_2-O_2-N_2$ flat flames providing small, slowly decaying residual radical pools. In the 1600–2000 K temperature range so investigated, HNO is stable enough against dissociation that catalysis is pronounced. Recombination of the surplus fragments occurs unaccompanied by noticeable diminution of the artificially added ($[NO] + [HNO]$) inventory through thermodynamically spontaneous but slower global reaction



The catalytic behavior of NO in the hypersonic combustion situation we modeled differs from that in the flat flame in several respects, in consequence of (i) the higher combustion temperature ($2400 < T < 3000$ K) we considered to precede expansion-induced recombination, and (ii) the significantly larger (forty-fold) fragment fraction (near 4% of the total flow, including N_2) to be recombined. The major effect is significant interruption of the catalytic cycle by frequent reversal of the bond-forming step (N4). The low net rate of (N4) becomes rate-limiting even as the larger H and OH populations make the HNO lifetime in steps (N5)/(N6) shorter than in the flat flame situation.

The second major difference, also primarily caused by the higher temperature range at which catalyzed recombination is needed in hypersonic combustion, is increased rates of the endothermic steps





of the extended Zeldovich chain. When that chain is completed by its rapid, exothermic step



there arises further need for recombination to accomplish reaction (N7).

Metal Oxide Catalysts

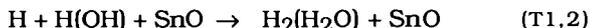
The other, and more promising class of recombination catalysts we have explored comprises partially oxidized forms of several metals, ranging in atomic weight from Mg to U. A survey was made [7] of twenty such metallic elements as part-per-million additives in atmospheric-pressure postflame gases near 1860 K. $\text{H}_2:\text{O}_2:\text{N}_2$ proportions were 3:1:6 and atom densities of $5 \times 10^{12} \text{ cm}^{-3}$ of each added metal were introduced as sprayed aqueous solution of a suitable salt. The largest catalytic effects [7], "2 orders of magnitude more effective than...NO...", occurred with the transition metals Cr, U, Sn and Mn. Similar catalysis also was found at 1860 K with the group II metals, Mg and the previously identified [8] heavier alkaline earths, Ca, Sr, and Ba. All these catalysts were further examined in hotter flames having lower proportions of N_2 , up to temperatures above 2400 K, where catalysis by the alkaline earth metals was significantly diminished. But, [7] "for Sn, Cr, and U (there was) no definite trend either up or down (over the 1800-2500 K range)." This finding implies that these metals will not lose their catalytic efficiency for promotion of recombination in the temperature regimes found in hypersonic ramjet propulsion.

For the group II elements and some if not all of the transition metals, catalytic sequences analogous to steps (4) - (6) are established.

In these, the analogs of O₂ and HO₂ are respectively, the strongly bound diatomic metal monoxide and the corresponding monohydroxide. Electronic states of the hydroxide other than its most strongly bound, ground state have been implicated in the catalytic sequence. Also, catalysis by involatile oxide particles is an incompletely resolved possibility for some of the transition metals, including Cr and U.

The flame chemistry and spectroscopy are more extensively studied [9] in the case of tin, and we chose this metal as the additive for modeling prospective catalyzed recombination in hypersonic combustion. In particular, SnO was shown to be the predominant species indistinguishable from 100% of the tin inventory. Even so, representation of the empirical catalysis by added Sn in postflame gases by means of elementary steps and their rate coefficients is uncertain.

Bulewicz and Padley [7] report an empirical rate constant, $k'_{\text{catalytic}}$ (k'_{cat}), for the global reactions



The k'_{cat} in this paper expresses the incremental contribution to the H-atom removal rate after subtraction of the terms from the uncatalyzed mechanism, representing the combined effect of steps (1) and (2) with H₂O, N₂ etc, as M. The rate coefficient was found to be

$$k'_{\text{cat}} \approx 5 \times 10^{-28} \text{ cm}^6 \text{ molecule}^{-2} \text{ s}^{-1} .$$

Allowance is included here for the stoichiometric factor of 2 between the rate of step (1) and the specific rate of reduction of the H-atom population. The mean of three k'_{cat} values above 2000 K is adopted. If the global reactions (T1,2) are assumed to be the elementary reaction steps for the catalytic mechanism a rate constant $k_{1,\text{SnO}}$ of this magnitude is unrealistically large.

Nevertheless, to assess the effectiveness of tin as a catalytic additive we incorporated into our kinetics model the reactions (T1,2).

With the addition of only 0.1% mole-fraction SnO of the total flow we realized an increase in the ideal combustion energy yield from the noncatalyzed 58% to 79%. This dramatic result compares to the equilibrium constrained result of nearly 100%.

The foregoing value of k'_{cat} is based on experience at $\leq 10^{-3}$ H-atom fraction in the flame gases, whereas early expansion of hypersonic combustion gases from a condition near 2900 K involved H-atom fraction up to 40 times larger. The consequent rate terms are thus extrapolated in our model to $\sim 10^3$ times larger magnitude. While this model indicated very strong catalysis its validity is uncertain.

As an alternative to using SnO as M in steps (1)-(4), the sequence:



has been postulated [7,9]. The superscript * denotes an electronically excited state of the monohydroxide molecule, SnOH.

Pursuing this catalytic sequence, steps (T4)-(T6) to represent the k'_{cat} in Ref. 7 paper, the deduced the equilibrium-constant ratio was

$$K_4 \equiv k_{\text{T4}}/k_{\text{-T4}} = 3 \times 10^{-18} \text{ cm}^3 \text{ molecule}^{-1}$$

and the rate coefficient was

$$k_{\text{T5}} \approx 2.6 \times 10^{-10} \text{ cm}^3 \text{ molecule}^{-1} \text{ s}^{-1}$$

When we have estimated individual values of $k_{T_4,M}$ and $k_{-T_4,M}$ for H_2O and N_2 , and M we find catalytic rates under hypersonic combustion conditions that are understandably smaller than by the k'_{cat} above, but not insignificant.

CONCLUSION

The more complete existing information on nonmetal oxides indicates that catalytic enhancement of combustion power by adding intentionally these materials will be unattractive, but the effects of constituents such as NO formed naturally from combustion in air are not negligible. However, the effects we predict based on the available literature data on metal oxides is encouraging. We conclude that further experimental investigation of volatile metallic additives as catalysts for recombination of H_2O fragments at high temperature, $T > 2400$ K, is advisable to advance the prospect of efficient, kinetically controlled enhancement of power for propulsion of hypersonic ramjets in circumstances where combustion would otherwise be thermochemically complete.

REFERENCES

1. Howard, C. J., "Kinetic Study of the Equilibrium $\text{HO}_2 + \text{NO} \rightleftharpoons \text{OH} + \text{NO}_2$ and the Thermochemistry of HO_2 ," *J. Am. Chem. Soc.* **1980**, *102*, 6937-6941.
2. Harradine, D., Lyman, J., Oldenborg, R., Schott, G., and Watanabe, H., "Hydrogen/Air Combustion Calculations: The Chemical Basis of Efficiency in Hypersonic Flows," *AIAA Preprint 88-2713*, **1988**, 7 pp; submitted to *AIAA J.*
3. Billig, F. S., "Combustion Processes in Supersonic Flow," *J. Propuls. Power* **1988**, *4*, 209-216.
4. Hanson, R. K. and Salimian, S., "Survey of Rate Constants in the H/N/O System;" *In Combustion Chemistry*, Gardiner, Jr., W. C., Ed.; Springer Verlag: New York, **1984**; Chapter 6.
5. Bulewicz, E. M. and Sugden, T. M., "Flame Photometric Studies of Reactions Induced by Nitric Oxide in Hydrogen-Oxygen-Nitrogen Flames. I. The Catalyzed Recombination of Atomic Hydrogen and Hydroxyl Radicals," *Proc. Roy. Soc. (London)* **1964**, *A277*, 143-154.
6. Halstead, C. J. and Jenkins, D. R., "Catalysis of Recombination Reactions in Flames by Nitric Oxide," *Chem. Phys. Lett.* **1968**, *2*, 281-2.
7. Bulewicz, E. M. and Padley, P. J., "Catalytic Effect of Metal Additives on Free Radical Recombination Rates in $\text{H}_2 + \text{O}_2 + \text{N}_2$ Flames." *Symp. (Int.) Combust. [Proc.]*, 13th **1971**, 73-80.
8. Cotton, D. H. and Jenkins, D. R., "Catalysis of Radical-Recombination Reactions in Flames by Alkaline Earth Metals," *Trans. Faraday Soc.* **1971**, *67*, 730-739.
9. Bulewicz, E. M. and Padley, P. J., "Photometric Observations on the Behavior of Tin in Premixed $\text{H}_2 + \text{O}_2 + \text{N}_2$ Flames," *Trans. Faraday Soc.* **1971**, *67*, 2337-2347.